J Neurophysiol 97: 3961–3975, 2007.
First published April 11, 2007; doi:10.1152/jn.00052.2007.

Voltage-Sensitive Conductances of Bushy Cells of the Mammalian Ventral Cochlear Nucleus

Xiao-Jie Cao, Shalini Shatadal, and Donata Oertel
Department of Physiology, University of Wisconsin School of Medicine, Madison, Wisconsin

Submitted 15 January 2007; accepted in final form 6 April 2007

Cao X-J, Shatadal S, Oertel D. Voltage-sensitive conductances of bushy cells of the mammalian ventral cochlear nucleus. *J Neurophysiol* 97: 3961–3975, 2007. First published April 11, 2007; doi:10.1152/jn.00052.2007. Bushy cells in the ventral cochlear nucleus convey firing of auditory nerve fibers to neurons in the superior olivary complex that compare the timing and intensity of sounds at the two ears and enable animals to localize sound sources in the horizontal plane. Three voltage-sensitive conductances allow bushy cells to convey acoustic information with submillisecond temporal precision. All bushy cells have a low-voltage-activated, α-dendrotoxin (α-DTX)-sensitive K^+ conductance (g_{KL}) that was activated by depolarization past –70 mV, was half-activated at –39.0 ± 1.7 (SE) mV, and inactivated ~60% over 5 s. Maximal g_{KL} varied between 40 and 150 nS (mean: 80.8 ± 16.7 nS). An α-DTX-insensitive, tetraethylammonium (TEA)-sensitive, K^+ conductance (g_{KH}) was activated at voltages positive to –40 mV, was half-activated at –18.1 ± 3.8 mV, and inactivated by 90% over 5 s. Maximal g_{KH} varied between 35 and 80 nS (mean: 58.2 ± 6.5 nS). A ZD7288-sensitive, mixed cation conductance (g_h) was activated by hyperpolarization greater than –60 mV and half-activated at –83.1 ± 1.1 mV. Maximum g_h ranged between 14.5 and 56.6 nS (mean: 30.0 ± 5.5 nS). 8-Br-cAMP shifted the voltage sensitivity of g_h positively. Changes in temperature stably altered the steady-state magnitude of I_h. Both g_{KL} and g_{KH} contribute to repolarizing action potentials and to sharpening synaptic potentials. Those cells with the largest g_h and the largest g_{KL} fired least at the onset of a depolarization, required the fastest depolarizations to fire, and tended to be located nearest the nerve root.

INTRODUCTION

Bushy cells receive information about the timing and fine structure of sounds from the temporal firing patterns in auditory nerve fibers and convey it to the superior olivary complex. Neurons in the MSO use phase-locking by large spherical bushy cells in the encoding of low-frequency sounds to compute the interaural phase and thus the relative time of arrival, of sounds at the two ears (Joris et al. 1998; Yin 2002). Neurons in the LSO compare the timing and frequency of excitation from ipsilateral small spherical bushy (Cant and Casseday 1986) and T (or planar) stellate cells (Doucet and Ryugo 2003) with inhibition from the medial nucleus of the trapezoid body (MNTB) that reflects the timing and frequency of firing of contralateral globular bushy cells in responses to high-frequency sounds to compute the relative intensities of sounds at the two ears (Tollin and Yin 2005; Yin 2002).

The three subtypes of bushy cells have been described in mammals that differ subtly in size and histological staining as well as in projection patterns: large spherical, small spherical, and globular bushy cells (Brawer et al. 1974; Cant and Casseday 1986; Cant and Morest 1979a,b; Osen 1969; Tolbert and Morest 1982a,b; Tolbert et al. 1982). Large spherical bushy cells in the rostral anterior VCN encode mainly low-frequency sounds and project to the lateral tuft in the ipsilateral and the medial tuft of dendrites of neurons in the contralateral MSO (Smith et al. 1993). Mice have little low-frequency hearing (Ehret 1974), a small and inconspicuous MSO and also few large spherical bushy cells (Willard and Ryugo 1983). In mice most bushy cells are of the globular and small spherical subtypes. Globular bushy cells are generally located near the root of the auditory nerve (Liberman 1991, 1993; Spirou et al. 1990; Tolbert and Morest 1982a,b; Tolbert et al. 1982), encode sounds of higher frequencies, and project to the MNTB through large axons that end in very large terminals, the calyces of Held (Brownell 1975; Liberman 1991; Sento and Ryugo 1989; Smith et al. 1991; Tolbert et al. 1982). Small spherical bushy cells are least well understood. Many project to the ipsilateral LSO, but it is unclear whether small spherical bushy cells or T stellate cells are the predominant source of ipsilateral excitation (Cant and Casseday 1986; Doucet and Ryugo 2003). Several lines of evidence indicate that globular and small spherical bushy cells are distinct. First, individually labeled globular bushy cells do not innervate the LSO (Smith et al. 1991). Second, monosynaptic, ipsilateral excitation of the LSO is matched in timing with disynaptic, contralateral inhibition through the MNTB and is therefore likely to be mediated through more slowly conducting axons (Joris and Yin 1995). In cats, the axons of globular bushy cells have exceptionally large diameters, small spherical bushy cells presumably have axons of intermediate diameter, and axons of T stellate cells have small diameters (Brownell 1975; Joris 1996; Tolbert et al. 1982).

Early recordings showed that bushy cells fire only one or two action potentials at the onset, whereas stellate cells fire tonically in response to a suprathreshold depolarizing current pulse (Fujino and Oertel 2001; Oertel 1983; Schwarz and Puil 1997; Wu and Oertel 1984). It has been reported that although all bushy cells fire transiently when they are depolarized, some seem to fire more than just one or two action potentials and require smaller currents to reach threshold (Francis and Manis 2000; McGinley and Oertel 2006; Wang and Manis 2006). Is it possible that early recordings were from only one of the three subtypes of bushy cells?

The anatomical and biophysical specializations of bushy cells play an integral role in their function. Bushy cells are

Address for reprint requests and other correspondence: D. Oertel, Dept. of Physiology, University of Wisconsin School of Medicine, 1300 University Ave., Madison, WI 53706 (E-mail: oertel@physiology.wisc.edu).

The costs of publication of this article were defrayed in part by the payment of page charges. The article must therefore be hereby marked "*advertisement*" in accordance with 18 U.S.C. Section 1734 solely to indicate this fact.

innervated by a small number of auditory nerve fibers through large terminals, the end bulbs of Held (Brawer and Morest 1975; Liberman 1991; Sento and Ryugo 1989). Activation of end bulb synapses produces large and rapid synaptic currents that produce rapidly rising and falling excitatory postsynaptic potentials (EPSPs) in bushy cells (Oertel 1983; Oleskevich and Walmsley 2002; Oleskevich et al. 2000; Rhode et al. 1983; Smith and Rhode 1987; Zhang and Trussell 1994). Bushy cells can encode and convey information about the fine structure of sounds because their EPSPs are brief and sharply timed (Joris et al. 1998; Kopp-Scheinpflug et al. 2002; Rhode et al. 1983; Smith et al. 1987, 1993; Winter and Palmer 1990). The brevity and sharp timing of synaptic responses are made possible by the low input resistance and concomitant short membrane time constants, τ_m, of bushy cells (Oertel 1983; Wang and Manis 2006; Wu and Oertel 1984). Temporally precise signals are brought to bushy cells by primary auditory neurons that have a short τ_m (Mo and Davis 1997a). The temporal precision is preserved in pathways to the MSO and to the LSO through the MNTB.

The earliest recordings from bushy cells indicated that the voltage-sensitive conductances that gave them short τ_m's in the physiological voltage range were critical for their ability to encode timing (Oertel 1983; Wu and Oertel 1984). Later work suggested that a low-voltage-activated potassium conductance, g_{KL}, coexists with a high-voltage-activated potassium conductance, g_{KH}, to provide the short τ_m's (Manis and Marx 1991). Indeed g_{KL} is present in many neurons at early stages of the auditory pathway (Bal and Oertel 2001; Dodson et al. 2002; Forsythe and Barnes-Davies 1993; Golding et al. 1995; Kuba et al. 2002, 2005; Mo et al. 2002; Rathouz and Trussell 1998; Reyes et al. 1994; Rothman and Manis 2003c; Scott et al. 2005; Wu 1999; Wu and Kelly 1995; Zhao and Wu 2001). Most of these neurons also have a hyperpolarization-activated, mixed cation conductance, g_h, the partial activation of which at rest also contributes to the short τ_m (Chen 1997; Cuttle et al. 2001; Leao et al. 2005, 2006; Mo and Davis 1997a). We show here that g_{KL}, g_{KH}, and g_h are prominent in bushy cells. The maximal values of g_{KL}, and g_h vary over a factor of about four and are correlated to transience in firing.

METHODS

Preparation of slices

Recordings were made from coronal slices of the most caudal region of the cochlear nuclear complex from mice (ICR strain) between 18 and 21 days old. They were cut in normal physiological saline that contained (in mM) 130 NaCl, 3 KCl, 1.2 KH_2PO_4, 2.4 $CaCl_2$, 1.3 $MgSO_4$, 20 $NaHCO_3$, 3 HEPES, and 10 glucose, saturated with 95% O_2-5% CO_2, pH 7.3–7.4, at between 24 and 27°C. The osmolality, measured with a 3D3 Osmometer (Advanced Instruments, Norwood, MA), was 306 mOsm/kg. All chemicals were from Sigma, unless stated otherwise. Slices, 200 μm thick, were cut with a vibrating microtome (Leica VT 1000S). Good recordings were most common in slices that were cut approximately in a coronal plane. The cut was tipped by ~30° from the coronal so that the dorsal part of the slice was more anterior than the ventral part of the slice. After cutting, slices were transferred to the recording chamber (~0.6 ml) and superfused continually at 5–6 ml/min. The temperature was measured in the recording chamber, between the inflow of the chamber and the tissue, with a Thermalert thermometer (Physitemp) the input of which comes from a small thermistor (IT-23, Physitemp, diameter: 0.1 mm). The output of the Thermalert thermometer was fed into a custom-made, feedback-controlled heater that heated the saline in glass tubing (1.5 mm) just before it reached the chamber to maintain the temperature at 33°C. An adjustable delay in the controller for the heater prevented oscillations. Slices were mounted on the stage of a compound microscope (Zeiss Axioskop) and viewed through a ×63 water-immersion objective. Recordings were generally made within 2 h after slices were cut.

Electrophysiological recordings

Patch-clamp recordings were made with pipettes of borosilicate glass the resistances of which ranged between 4 and 6 MΩ. They were filled with a solution consisting of (in mM) 108 potassium gluconate, 9 HEPES, 9 EGTA, 4.5 $MgCl_2$, 14 phosphocreatinine (Tris salt), 4 ATP (Na salt), and 0.3 GTP (tris salt) that had a final osmolarity 297 mOsm/kg. The pH was adjusted to 7.4 with KOH. Recordings were made with an Axopatch 200A amplifier (Axon Instruments). Records were digitized at 50 kHz and low-pass filtered at 10 kHz. All reported results were from recordings in which 80~90% of the series resistance could be compensated on-line with 10 μs lag; no corrections were made for errors in voltage that resulted from uncompensated series resistance. The series resistance was 11.8 ± 0.7 MΩ (n = 60). With a cell capacitance 26.0 ± 2.6 pF, the time constant of the imposed voltage step was therefore ≥35 μs; recordings with changes in series resistance exceeding 2 MΩ were excluded from analysis. The output was digitized through a Digidata 1320A (Axon Instruments) and fed into a computer. Stimulation and recording was controlled by pClamp 8 software (Axon Instruments). The control solution contained (in mM) 138 NaCl; 4.2 KCl, 2.4 $CaCl_2$, 1.3 $MgCl_2$, 10 HEPES, and 10 glucose, pH 7.4, 306 mOsm/kg, and saturated with 100% O_2. In voltage-clamp experiments, the voltage-sensitive sodium current was blocked by 1 μM tetrodotoxin (TTX), the voltage-sensitive calcium current was blocked by 0.25 mM $CdCl_2$, glutamatergic and glycinergic synaptic currents were blocked with 40 μM 6,7-dinitroquinoxaline-2,3-dione (DNQX) (Tocris Cookson, UK) and 1 μM strychnine respectively. In some experiments, 50 μM ZD7288, 10 mM TEA, or 50 nM α-DTX (Bal and Oertel 2000), were added to the control solution to isolate the I_{KL}, I_{KH}, and I_h. All reported voltages were compensated for a –12-mV junction potential.

Data analysis

The measurements of conductance from individual cells was fitted by a Boltzmann equation, $g/g_{max} = 1 - 1/[1+\exp(V - V_{1/2})/\kappa]$. Statistical analyses were made with Origin software (version 7.5); the results are given as means ± SE with n being the number of cells in which the measurement was made.

Histology

In some experiments, the physiological identification of bushy cells was verified anatomically. In these experiments, 0.1% biocytin was included in the pipette solution, and slices were fixed with 4% paraformaldehyde immediately after the recording. When the pipette was removed from the cell before fixation, even when fixation was initiated within seconds, cells were almost always damaged, leaving only clusters of labeled beads or beaded processes. To avoid such damage, fixative was introduced into the recording chamber for 5–10 min before the pipette was removed from the cell. Although the cell body and some processes were still sometimes lost, either torn away by the pipette or in the histological processing, the morphology of dendrites and the long stretches of straight axons show that these cells were well fixed even when some parts were lost. Slices were stored in 4% paraformaldehyde at 4°C. Before processing they were embedded in a block of gelatin and albumin that was cross-linked with glutaraldehyde and sectioned at 60 μm in the plane of the slice with a

vibratome. Slices were incubated with avidin conjugated to horseradish peroxidase (Vector ABC kit, Vector Laboratories, Burlingame, CA), and cells were visualized after processing for horseradish peroxidase with cobalt and nickel intensification (Zhang and Oertel 1993). The sections were mounted on subbed slides, and counterstained with cresyl violet. Labeled cells were reconstructed with a camera lucida using a ×100 objective and digitized. To measure the distances of labeled cells from the nerve root, the outlines of the coronal sections of the VCN, the locations of the labeled cell, the granule cell areas and the nerve root were reconstructed using a ×10 objective and collapsed in the rostrocaudal dimension. The distance between the cell body and the nearest part of the root of the auditory nerve were measured in the coronal plane. We did not compensate for distance in the rostrocaudal dimension evident when labeled cells were not in the same sections as the nerve root because such compensation was approximate and affected the results only subtly.

RESULTS

Bushy cells have characteristic responses to current pulses

This study was based on 129 current- and voltage-clamp recordings. Of these, 69 were recorded with biocytin-filled pipettes and 24 were recovered and identified anatomically. Figure 1 shows reconstructions of eight of the labeled bushy cells. They are shown together with their responses to 0.4-nA depolarizing and 0.6-nA hyperpolarizing current pulses. Bushy cells characteristically have one or two primary dendrites that branch profusely in a bush of short dendrites. Dendrites in every cell were uneven in thickness; thickenings in dendrites of bushy cells presumably hold clumps of mitochondria (Cant and Morest 1979b). The axons of bushy cells were labeled for varying distances; in three cases, they could be followed into the trapezoid body (Fig. 1*C*). Axons were generally narrow where they emanated from the cell body and then widened. Responses to injected current follow a consistent pattern. Depolarizing current pulses evoked one or two action potentials that were followed by a small, flat depolarization in some bushy cells as was described previously (Fig. 1, *D, F,* and *G*) (Francis and Manis 2000; Leao et al. 2005, 2006; Oertel 1983; Wang and Manis 2006; Wu and Oertel 1984), but in others, depolarization evoked more action potentials and oscillations in voltage at the onset of a current pulse and even an occasional action potential in the middle of a pulse (Fig. 1, *A–C, E,* and *H*), a pattern that has not previously been observed in anatomically identified bushy cells. In every cell, the first action potential reached a more depolarized peak, to between –20 and 0 mV, than those that followed. Hyperpolarizing current pulses produced relatively larger voltage changes that sagged back toward rest. The shapes of the sags were variable. In some cells, sags were deep and relatively rapid (Fig. 1, *A, D, F,* and *G*), whereas in others, the sags were slower and less deep (Fig.

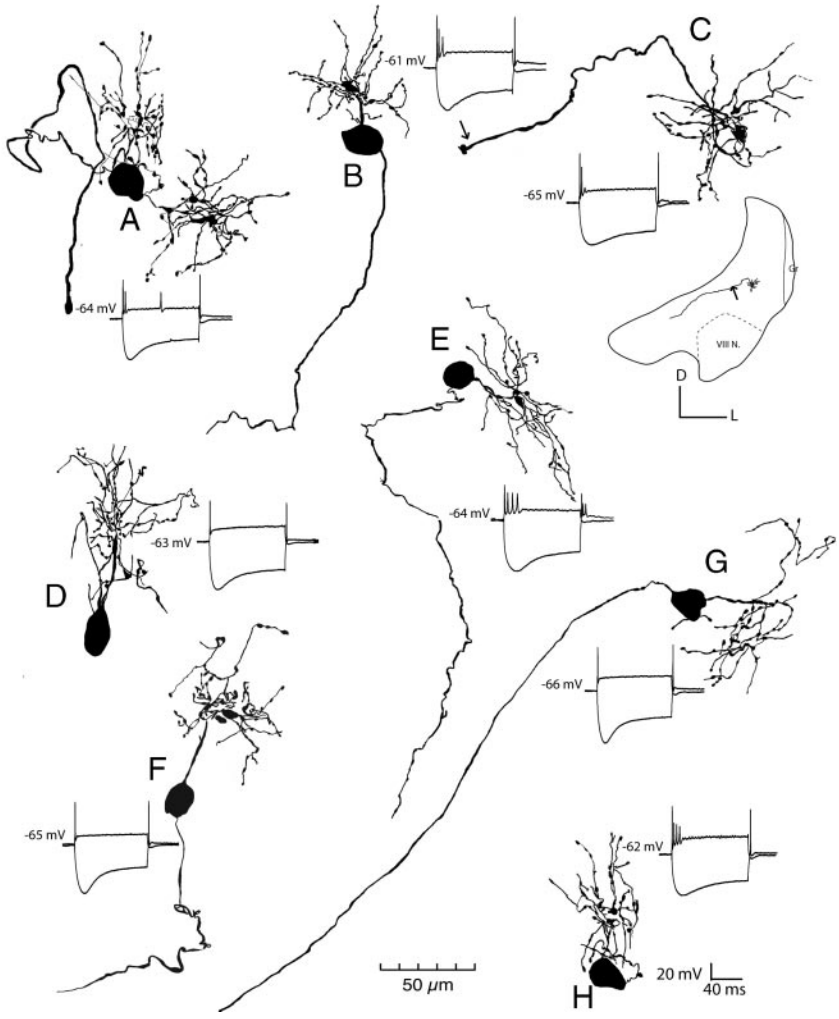

FIG. 1. Bushy cells have characteristic responses to current. Reconstructions of eight of the labeled bushy cells and their responses to 0.4-nA depolarizing and –0.6-nA hyperpolarizing current pulses show that each cell has the characteristic bush of short, thin, beaded dendrites and that each fires only transiently at the onset of a depolarization. The axon of cell C could be followed into the trapezoid body as shown in the reconstruction of the tissue slice in the *inset*; →, corresponding points of the axon. The dendrites of this cell identified the cell as a bushy cell, but the cell body, necessarily near a surface in patch-clamp recordings, was lost in the histological processing. The traces show the current clamp recorded from labeled bushy cells in AVCN. Depolarizing current pulses evoked a single action potential in some bushy cells (*D, F, G*) and a few action potentials in others (*A, B, C, E, H*). The 1st action potential consistently reached a higher peak than subsequent ones. Hyperpolarizing current pulses evoked responses that sagged quickly (*A, D, F, G*) or slowly (*B, C, E, H*) back toward rest.

1, *B, C, E,* and *H*). The pattern is consistent with that described with sharp-electrode recordings earlier although some of the bushy cells fired more action potentials at the onset of a depolarization than was described before (Francis and Manis 2000; Oertel 1983; Wu and Oertel 1984). In no case was a cell with this pattern of responses found not to be a bushy cell when it was labeled anatomically. These findings confirm that transient firing is an identifying characteristic of bushy cells but also show that depolarizing current pulses can evoke more than just one or two action potentials.

It is possible that the subtle differences in responses to current reflect differing subtypes of bushy cells because bushy cells near the root of the auditory nerve tended to respond to depolarizing current pulses with few action potentials followed by a flat depolarization and to hyperpolarization with deep sags whereas those recorded somewhat more dorsally were more likely to fire more action potentials and have slower, shallower sags. To document differences in location, the distance from the auditory nerve in the coronal plane was plotted as a function of the maximum number of action potentials (Fig. 2). The plot shows that while differing types of bushy cells are intermingled, there was a correlation between firing patterns and their location. The r^2 value of the linear regression was 0.22, showing that the trend is statistically significant ($P < 0.05$) even in the absence of the cell with the largest number of action potentials, linear regression showed a significant correlation with $r^2 = 0.18$ and $P < 0.05$.

Firing in response to depolarizing current has served as an identifying characteristic of bushy cells and was therefore explored further. Most bushy cells fired only a single action potential at the onset of a depolarization, independent of the strength of the current (Figs. 1, *D, F,* and *G,* and 3, *A* and *B,* ○). In others, however, increasing current evoked first more, reached a maximum, and then fewer action potentials (Fig. 3*B,* △). On average, bushy cells fired maximally when they were depolarized with 0.6 nA (Fig. 3*B,* ■).

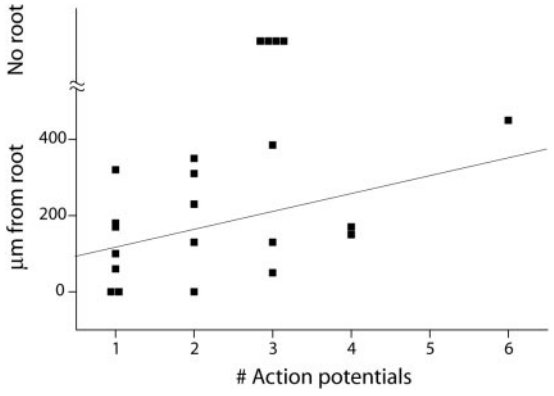

FIG. 2. Bushy cells that fired maximally few action potentials tended to lie nearer the nerve root than those that fired more. The nerve root is visible and has a distinct border in Nissl-stained sections as an area in which stained cell bodies line up between unstained fascicles of auditory nerve fibers. Measurements of the distance between labeled cell bodies and the nerve root show that there is a correlation between the maximum number of action potentials that bushy cells fired and the distance from the nerve root. Linear regression, indicated by the line with $r^2 = 0.22$, shows that there is a statistacally significant correlation between firing properties and position in the nucleus ($P < 0.05$). Even in the absence of the cell that fired 6 action potentials, the linear regression showed a significant correlation with $r^2 = 0.18$ and $P < 0.05$.

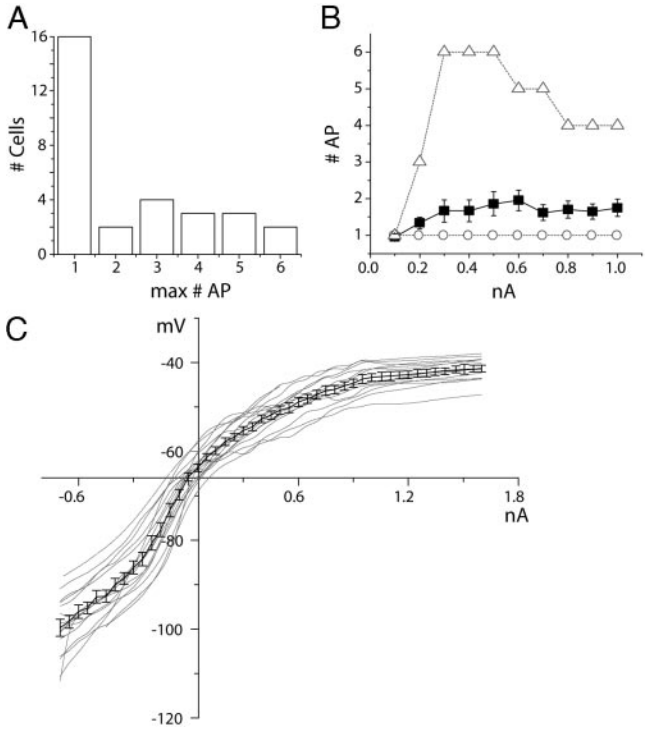

FIG. 3. Responses of bushy cells to injection of current reveal characteristic patterns of firing and rectification in both the depolarizing and hyperpolarizing voltage ranges. *A*: bar graph shows that depolarization with current evoked only a single action potential in about half of the cells sampled. In the other cells current evoked between 2 and 6 action potentials. *B*: plot shows number of action potentials fired as a function of injected depolarizing current. ○, cell that fired only a single action potential when it was depolarized with suprathreshold currents between 0.1 and 1.0 nA. △, how the number of action potentials varied nonmonotonically as a function of injected current in a cell that fired maximally 6 action potentials. The maximum number of action potentials was evoked by currents between 0.3 and 0.5 nA in the population of recorded cells. ■, average number of action potentials as a function of injected current in 30 bushy cells. *C*: plots of voltage as a function of injected current show rectification in both the depolarizing and hyperpolarizing voltage range. The slope of these plots at the resting potential is their input resistance, on average 67.2 ± 17.1 MΩ ($n = 36$).

The second identifying characteristic of bushy cells is the rectification in the voltage/current relationship in the depolarizing voltage range. A plot of the voltage changes at the end of 100-ms current pulses as a function of the strength of the injected current reveals rectification in the depolarizing voltage range in every cell (Fig. 3*C*). The slope of the *V-I* relationship at rest, a measure of the input resistance, was on average 67.2 ± 17.1 MΩ ($n = 36$). The sigmoid shape reflects the presence of noninactivating, voltage-sensitive conductances in both depolarizing and hyperpolarizing voltage ranges.

Tonic firing in bushy cells is prevented by an α-DTX-sensitive conductance. Recordings in Fig. 4 (*left*) show how three bushy cells responded to depolarizing current with transient, firing. One of these cells fired occasionally after the initial transient (Fig. 4*Ab*). The application of 50 nM α-DTX depolarized every bushy cell tested by between 2 and 4 mV and enabled it to fire tonically (Fig. 4*B*) independently of whether the cell fired only once (Fig. 4, *a*) or multiple times (Fig. 4, *c*). (The traces shown in Fig. 4*B* were recorded after bushy cells were brought back to their original resting potentials with hyperpolarizing current.) Even in the presence of α-DTX, the first action potential was larger than later ones. Large depolar-

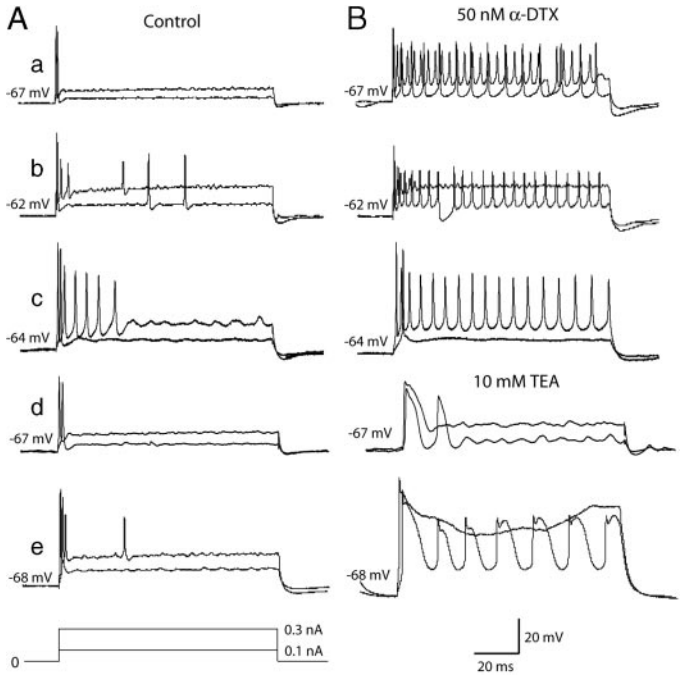

FIG. 4. The α-DTX-sensitive and TEA-sensitive K^+ conductances control differing facets of firing. *A*: superimposed responses to identical depolarizing current pulses, 0.1 and 0.3 nA, show characteristic, transient firing. Cell shown in *a* fired only once whereas others fired multiple action potentials. In some cells, action potentials were followed by membrane oscillations. In the cell shown in *b*, those oscillations were occasionally suprathreshold. The magnitude of the steady depolarization toward the end of the current pulses varied between cells reflecting differences in the input resistance. The cell shown in *a* had the lowest input resistance and the most rapid repolarization after the end of the pulse. The cell shown in *e* had the highest input resistance and the slowest repolarization. *B*: application of blockers of K^+ conductances caused changes in the firing pattern. 50 nM α-DTX, a blocker of low-voltage-activated K^+ conductances, depolarized each of the cells tested by 2–4 mV and enabled them to fire tonically for the duration of the current pulse. The traces in *B* were recorded when the resting potential was returned to the same level as in *A* by a steady, hyperpolarizing current. In the presence of α-DTX, firing could be transient in responses to small (*c*) or large (*b, d*) currents, and the initial action potential remained taller than subsequent ones. Commonly, prominent inhibitory postsynaptic potentials (IPSPs) were observed in the presence of α-DTX (*a, b*), indicating that inhibitory interneurons had α-DTX-sensitive conductances. 10 mM TEA, in contrast, lengthened the duration of action potentials (*d, e*), indicating that action potentials in bushy cells are repolarized by TEA-sensitive conductances.

izations resulted in a depolarization block in some bushy cells (Fig. 4*Bb*). Action potentials were broadened slightly (duration at threshold in responses to 0.1 nA in control conditions 1.7 ± 0.4 ms, α-DTX 2.4 ± 0.7 ms, $n = 10$), but their peaks did not change when α-DTX was applied (responses to 0.3 nA under control conditions 32.4 ± 2.7 mV, with α-DTX 33.1 ± 1.9 mV, $n = 11$). In the presence of α-DTX, prominent IPSPs were sometimes observed (Fig. 4*B, a* and *b*), suggesting that inhibitory interneurons have an α-DTX-sensitive K^+ conductance. In contrast, the application of 10 mM TEA resulted in the broadening (duration at threshold in responses to 0.1 nA in control conditions 1.1 ± 0.1 ms, TEA 7.4 ± 2.9 ms, $n = 5$) and heightening of action potentials (responses to 0.3 nA under control conditions 36.9 ± 4.9 mV, with TEA 41.9 ± 8.6 mV, $n = 6$, Fig. 4, *d* and *e*).

Hyperpolarizing current causes a large hyperpolarization that sags back toward rest in bushy cells. The shape of the sag showed considerable variability in that the voltage sagged more quickly and more deeply in some cells than others (Figs. 1 and 5*A*). The sag toward rest could be reasonably well fit with a single-exponential function; the depth of the sag was quantified as the ratio between steady-state and peak voltage changes. Figure 5*B* shows that there was a positive correlation between the rate of the sag and its depth in responses to 0.8-nA hyperpolarizing current pulses in 40 bushy cells; in some cells the sag was deep (small b/a) and rapid (small τ_h), whereas in others, it was slower and less deep. The time course, and therefore also the depth of the sag, was correlated with the maximum number of action potentials elicited by depolarizing current pulses (Fig. 5*C*). Cells with the slowest and shallowest sags fired the most action potentials. Fifty micromolars

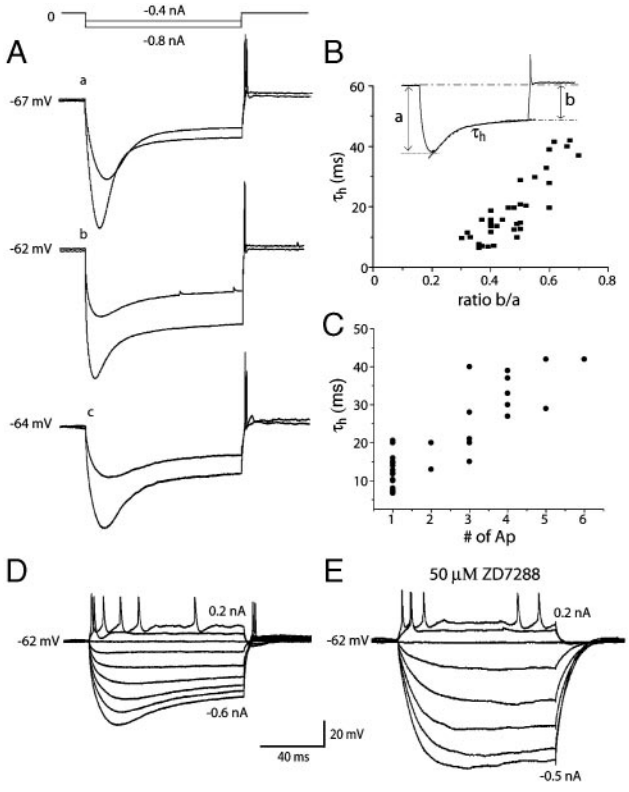

FIG. 5. Responses of bushy cells to hyperpolarizing current pulses sag back toward rest, showing inward rectification. *A*: voltage responses to identical hyperpolarizing current pulses in the same 3 bushy cells the responses of which to depolarization are illustrated in Fig. 4, *a–c*, show considerable variability. Peak hyperpolarizations were larger in some cells (*a, b*) than in others (*c*), the rates and depths of the sags were also larger in some cells (*a*) than in others (*b, c*). After the offset of hyperpolarizing current pulses, all bushy cells responded with anode-break action potentials. *B*: to compare features of the sag between bushy cells, the time course and depth of sags were compared in responses to −0.8 nA. *Inset*: depth of the sag was measured as the ratio between the steady-state (b) and peak hyperpolarization (a). The time course of sags was assessed by fitting with a single exponentials the time constant of which is τ_h. The plot summarizes results from 40 bushy cells and shows that the time course and depth of sags are correlated; cells with the most rapid sags toward rest (short τ_h) had deepest sags (small b/a). *C*: responses to hyperpolarizations were further correlated with responses to depolarization. Those bushy cells with the slowest sags responded to depolarizing current with the largest maximum number of action potentials. *D*: responses to depolarizing and hyperpolarizing current pulses show transient firing and a sag toward rest. *E*: in the same cell the responses of which are shown in *D,* the blocker of hyperpolarization-activated conductances, ZD7288, reduced the sag, and increased the input resistance in the hyperpolarizing voltage range but had little effect on the shape or temporal pattern of action potentials.

ZD7288 blocked the sag but did not affect the firing of bushy cells (Fig. 5, *D* and *E*, $n = 4$).

Measurement of voltage-sensitive conductances

To examine the voltage-dependent conductances that give bushy cells their characteristic properties, conductances through different populations of ion channels were separated from one another and studied under voltage clamp. In voltage-clamp experiments, 1 μM TTX and 0.25 mM Cd^{2+} were added to the extracellular bathing solution to block Na^+ and Ca^{2+} inward currents. In these experiments, spontaneous glutamatergic and glycinergic synaptic currents were also routinely blocked with 40 μM DNQX and 1 μM strychnine. As the voltage range of activation of g_{KL} overlaps those of g_{KH} and g_h, one of each of the pairs of conductances had to be blocked to study the other. Fifty micromolars ZD7288 was used to block g_h and 50 nM α-DTX to block g_{KL}.

Low-voltage-activated K^+ conductance (g_{KL})

The characteristics of g_{KL} are illustrated in Fig. 6. Measurements of this conductance were made in the presence of 1 μM TTX, 0.25 mM Cd^{2+}, 50 μM ZD7288, 40 μM DNQX, and 1 μM strychnine to block g_{Na}, g_{Ca}, g_h, and glutamatergic and glycinergic synaptic currents, respectively. From a holding potential of −80 mV, voltage pulses more depolarizing than −70 mV evoked outward currents whose rise was too rapid to be resolved from the capacitative transient in every bushy cell tested (Fig. 6*A*). Plots of peak outward currents as a function of voltage show that currents were activated at about −70 mV (Fig. 6*B*). As these currents are activated at relatively hyperpolarized potentials, they were dubbed low-voltage-activated currents (I_{KL}). Although the voltage sensitivity of I_{KL} was consistent between bushy cells, the magnitude of the current varied over a fourfold range (Fig. 6*B*, $n = 14$).

The reversal potential of I_{KL} was determined from the reversal of tail currents. A voltage pulse to −50 mV was used to activate g_{KL}. Tail currents were then measured with subsequent voltage pulses to between −60 and −110 mV. I_{KL} reversed at −80.0 ± 3.1 mV ($n = 6$), near the theoretical equilibrium potential for K^+, −85 mV.

At potentials more depolarized than −40 mV, not only I_{KL} but also I_{KH} were activated so that the two currents had to be separated pharmacologically as shown in Fig. 6*C–E*, to be studied. A family of voltage steps from −80 to +20 mV evoked a substantial outward current. The application of 50 nM α-DTX reduced the evoked outward current. Subtracting currents evoked in the presence of α-DTX from those under control conditions separated the α-DTX-insensitive current (Fig. 6*D*) from the α-DTX-sensitive current (Fig. 6*E*). The current that was blocked by α-DTX activated near −70 mV whereas that which remained after the application of α-DTX activated at voltages more depolarized than about −40 mV, indicating that α-DTX blocked essentially all of I_{KL} and could be used to separate I_{KL} from I_{KH} (Fig. 6*F*). The clustering of currents in responses to large depolarizations (Fig. 6*E*) and the curvature in the *I-V* plot (Fig. 6*F*) indicate that the voltage was not perfectly clamped in the presence of large outward currents. The measured currents were converted to conductance with Ohm's law, $g_{KL} = I_{KL}/(V_m - E_{rev})$ (Fig. 6*G*). The

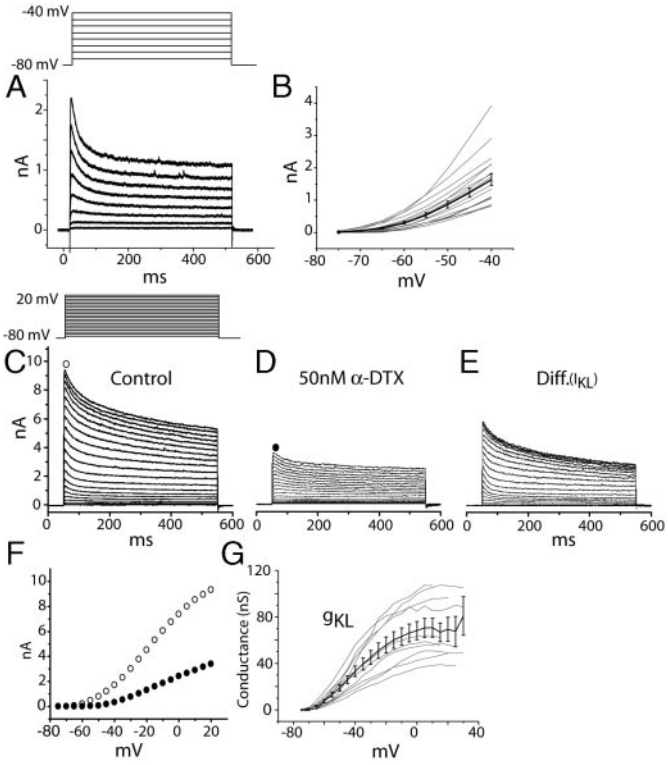

FIG. 6. Low-voltage-activated K^+ current and conductance in bushy cells. *A*: depolarizing voltage pulses, imposed from a holding potential of −80 mV in 5-mV steps to −40 mV, evoked voltage-sensitive outward currents. Those currents rose too rapidly to be resolved from the capacitative transient, reached a peak and then inactivated partially. *B*: peak outward currents rose as a function of voltage from about −70 mV. The magnitudes of currents varied among bushy cells, ranging from 0.6 to 2.9 nA at −45 mV and had an average of 1.2 ± 0.1 nA ($n = 14$). *C–E*: to measure the voltage sensitivity of I_{KL} over its entire range of voltage sensitivity required that I_{KL} be separated pharmacologically from I_{KH}. *C*: voltage pulses from −80 to +20 mV, presented in 5-mV steps, evoked mixed I_{KL} and I_{KH}. *D*: 50 nM α-DTX was added to the extracellular saline to block I_{KL}, and currents were measured in response to the identical voltage pulses as *C*. *E*: difference in currents recorded in the absence (*C*) minus those recorded in the presence of 50 nM α-DTX (*D*) represents the α-DTX-sensitive current. The clustering of currents in responses to large depolarizations (also reflected in the curvature of the *I-V* plot in *F*, ○) reflects imperfect clamping of the current. *F*: under control conditions, peak outward currents were activated at voltages more positive than about −70 mV (○), whereas the current that remained after the application of α-DTX (●) activated at voltages more positive than about −40 mV. *G*: voltage sensitivity of the activation of g_{KL} was measured from peak difference currents such as those illustrated in *E* by converting current to conductance with Ohm's Law. Maximum g_{KL} ranged from 38.8 to 107.0 nS, the mean maximal g_{KL} being 80.8 ± 16.7 nS ($n = 11$). All measurements were made in saline that contained 1 μM TTX, 0.25 mM Cd^{2+}, and 50 μM ZD7288 to suppress voltage-sensitive I_{Na}, I_{Ca}, and I_h, and 40 μM DNQX and 1 μM strychnine to block spontaneous glutamatergic and glycinergic synaptic currents.

maximal g_{KL} ranged between 40 and 140 nS among bushy cells and had a mean of 80.8 ± 16.7 nS ($n = 11$). Imperfections in clamping could make these underestimates of the maximal conductance. The sigmoidal, mean g_{KL} was fit by a Boltzmann function with half-activation at –37.6 ± 2.1 mV and a slope factor of 10.2 ± 1.0 mV ($n = 11$).

Pharmacological blockers give an indication of what subunits form g_{KL}. α-DTX blocks potassium channels of the Kv1 family that contain Kv1.1, Kv1.2, Kv1.3, and Kv1.6 α subunits (Dolly and Parcej 1996; Grissmer et al. 1994; Harvey 1997; Owen et al. 1997; Tytgat et al. 1995). DTX-K (40 nM), a blocker that is specific for channels that have Kv1.1 α subunits

(Owen et al. 1997; Robertson et al. 1996; Wang et al. 1999a,b), blocked 72.3 ± 6.4% (n = 4) of the peak I_{KL}. 100 nM Tityustoxin Kα, a blocker that is selective for Kv1.2 α subunits (Hopkins 1998; Werkman et al. 1993), blocked 57.8 ± 6.8% (n = 4) of the peak I_{KL} at −45 mV. The currents blocked by DTX-K and tityustoxin Kα are together >100%, indicating that part of the current is sensitive to both blockers and that these toxins do not define mutually exclusive currents. I_{KL} is thus mediated through heteromeric voltage-sensitive channels of the Kv1 family, some of which contain Kv1.1 α subunits and some of which contain Kv1.2 subunits. These results also show that α-DTX sensitivity can be used to separate I_{KL} from other currents, including I_{KH}.

High-voltage-activated K^+ conductance (g_{KH})

The high-voltage-activated current, I_{KH}, was defined by its insensitivity to α-DTX and its sensitivity to 10 mM TEA. In the presence of 50 nM α-DTX, voltage steps from a holding potential of −80 mV evoked outward currents that inactivated slowly (Fig. 7*A*). These currents were largely blocked by 10 mM TEA (Fig. 7*B*). The difference between these families of currents revealed the TEA sensitive, α-DTX-insensitive current, I_{KH} (Fig. 7*C*). The clustering of currents in responses to large depolarizations indicates that the currents were not perfectly clamped at the highest voltages. The g_{KH} in a group of bushy cells is shown in Fig. 7*D*. It becomes activated when bushy cells are depolarized more than about −45 mV. The maximum conductance, g_{KHmax}, varied by a factor of about two and had a mean 58.2 ± 6.5 nS (n = 12). Fitting the average g-V relationship with a Boltzmann function showed that g_{KH} was half activated at –18.4 ± 1.9 mV and had a slope factor of 8.7 ± 0.9 mV (n = 12).

The reversal potential for g_{KH} was measured from tail currents in the presence of α-DTX. I_{KH} reversed at –77.0 mV ±3.4 mV (n = 4). The difference between the reversal potentials of I_{KH} and I_{KL} was not statistically significant (Student's t-test, P = 0.24).

Several groups have reported the presence of A-type K^+ conductances, conductances that are strongly inactivated near the resting potential, in cochlear nuclear cells (Rathouz and Trussell 1998; Rothman and Manis 2003a). In recordings from bushy cells, the magnitude of peak outward currents was not significantly affected by varying the holding potential between –70 and –90 mV (n = 3). We have observed A-type K^+ conductances in other cells but never in a bushy cell.

Hyperpolarization-activated conductance (g_h)

Hyperpolarizing voltage steps evoked a slowly activating and slowly deactivating inward current in bushy cells. To isolate I_h, recordings were made in the presence of 10 mM TEA, 50 nM α-DTX, 0.25 mM Cd^{2+}, 1 μM TTX, 40 μM DNQX, and 1 μM strychnine. Control experiments showed that I_h was not significantly affected by the cocktail of drugs (data not shown). Figure 8*A* shows a family of inward currents that was evoked by hyperpolarizing voltage pulses. Immediately after the capacitative transient, there was an "instantaneous" change in current, which reflected current flowing through the resting conductance of the cell just before the voltage step. The inward current then increased slowly to a steady state, reflecting the activation of g_h. After the capacitative transient at the end of the voltage step, the current declined back to the original holding level in a current tail as I_h deactivated. The bradicardiac agent, ZD7288, has been shown to block I_h selectively in many types of neurons including in neurons of the ventral cochlear nucleus (Bal and Oertel 2000; Maccaferri and McBain 1996). In bushy cells that were bathed in a cocktail of blockers, addition of 50 μM ZD7288 reduced the instantaneous current by 76.0 ± 2.7% (n = 8), prevented much of the slow activation of the inward current and substantially reduced the tail current. These results show that ZD7288 blocked most of the current, although some time- and voltage-dependent unblocking is evident as has also been observed in other types of neurons (Harris and Constanti 1995; Shin et al. 2001). I_h is inward even around rest, consistent with its being a mixed cation current. Plots of the I-V curve of steady-state currents in bushy cells are shown in Fig. 8*B*. Their magnitudes differed over a fivefold range among bushy cells. The reversal potential for I_h was measured as the point where chord conductances intersect (Bal and Oertel 2000). The mean reversal potential of I_h was −40.8 ± 2.3 mV (n = 5). The voltage sensitivity of g_h was measured from tail currents after a family of voltage steps that encompassed the voltage range over which

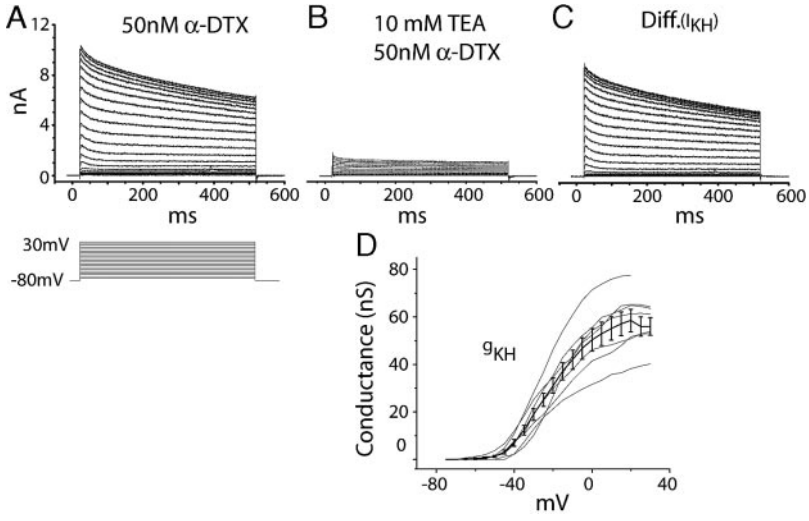

FIG. 7. I_{KH} was defined as the current that is insensitive to α-DTX and sensitive to 10 mM TEA. *A*: in the presence of 50 nM α-DTX, currents were evoked with depolarizing steps from −80 to +30 mV. *B*: in the same cell, currents to similar voltage pulses were evoked in the additional presence of 10 mM TEA. *C*: difference between currents in *A* and *B* reveals the TEA-sensitive, α-DTX-insensitive current that is defined as I_{KH}. *D*: current values were converted to conductance, g_{KH}, using –77 mV as the reversal potential. The mean maximal conductance, g_{KHmax}, was 58.2 ± 6.5 nS (n = 12). The measurements described in this figure were made in the presence of 1 μM TTX, 0.25 mM Cd^{2+}, 50 μM ZD7288, 40 μM DNQX, and 1 μM strychnine to block g_{Na}, g_{Ca}, g_h, and glutamatergic and glycinergic synaptic currents.

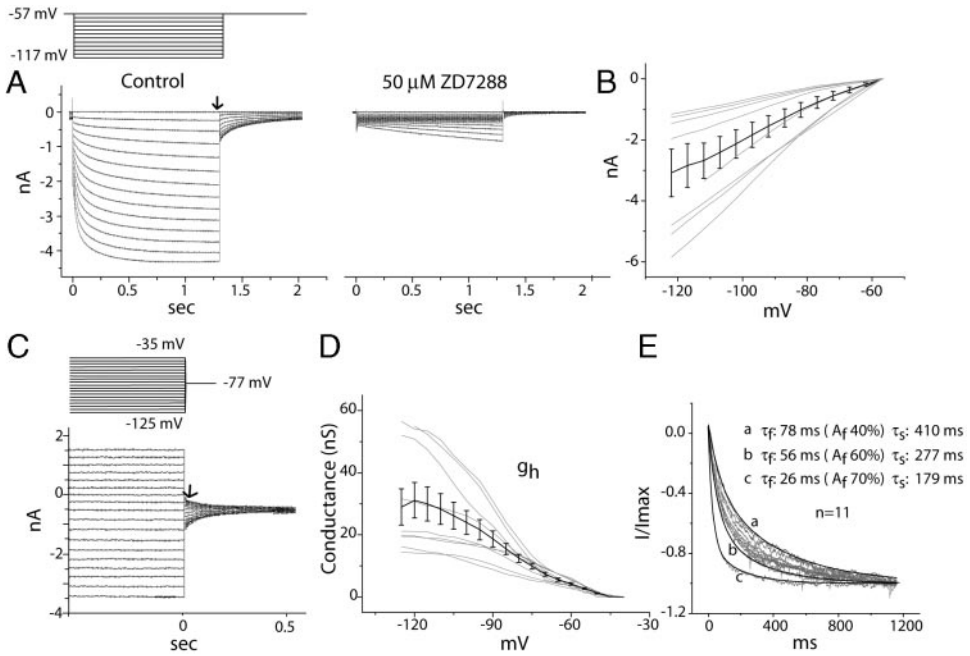

FIG. 8. Hyperpolarization activates a ZD7288-sensitive current, I_h. *A*: voltage steps from –57 to –117 mV in 5-mV increments elicited first an instantaneous and then a slowly activating, inward current in a bushy cell. Adding 50 μM ZD7288 to the bath reduced the instantaneous current and eliminated the slowly activating current. In the presence of ZD7288 and at strongly hyperpolarized voltages, some unblocking was evident that increased with time. *B*: plots show the relationship between voltage and steady-state currents ($\downarrow$ in *A*) in a population of 9 bushy cells. *C*: voltage sensitivity of g_h was derived from tail currents. The potential was first stepped from –62 mV to voltages that encompassed the entire range of voltage sensitivity of I_h, between –35 and –125 mV for 1.3 s (of which only the final 0.5 s is shown). The extent of activation was assayed at –77 mV, near the reversal potential of I_{KL} and I_{KH}. The amplitudes of the tail currents ($\downarrow$ in *C*) reflected the conductance activated by the preceding voltage pulse. *D*: relationships of conductance as a function of voltage for 10 experiments and averaged show that the maximum conductance varied. The maximum g_h ranged from 14.5 to 56.6 nS and had an average of 30.0 $\pm$ 5.5 nS (n = 10). A Boltzmann fit to the averaged conductance (solid black line) had $V_{1/2}$ = –83.1 $\pm$ 1.1 mV and a slope factor k = 9.9 $\pm$ 1.1 mV. *E*: rates at which I_h activated, varied between cells. To compare activation rates, currents evoked by pulses to –112 mV in 11 bushy cells were superimposed. Instantaneous currents were subtracted and the magnitude of currents was normalized to the current activated at the end of a 2-s pulse; only the 1st 1,200 ms of the 2-s pulses are shown. Most rates fell between a and b but I_h activated more rapidly in one cell. All experiments were done in the presence of a cocktail of blockers of other conductances, 10 mM TEA, 50 nM α-DTX, 0.25 mM Cd^{2+}, 1 μM TTX, 40 μM DNQX, and 1 μM strychnine.

g_h is affected by voltage. The activation of g_h at the steady state by the family of voltage steps was reflected in the amplitude of tail currents on return to –77 mV after steps to voltages between –35 to –125 mV (Fig. 8*C*, $\downarrow$). The tail current when the voltage was stepped from a variable voltage to –77 mV reflects a change in activation of g_h. This tail current reflects a deactivation when the voltage is stepped from more hyperpolarizing potentials to –77 mV and activation of I_h when the voltage is stepped from more depolarizing potentials to –77 mV (Fig. 8*C*). The tail currents saturated at large hyperpolarizing test potentials, as g_h approached its maximum value and at depolarized potentials as g_h approached the minimum. The relative amplitude of tail currents, measured immediately after the relaxation of the capacitative transient, is plotted in Fig. 8*D*. This plot shows the voltage sensitivity of g_h in 10 bushy cells. The values of g_h were derived from the absolute values of tail currents $g_h(V) = (I - I_{min})/(V_m - E_{rev})$ and plotted as a function of the voltage of the preceding step (V_m). The maximum g_h ranged from 14.5 to 56.6 nS and had an average of 30.0 $\pm$ 5.5 nS (n = 10) in bushy cells (Fig. 8*D*). A Boltzmann fit to the averaged activation curve gave $V_{1/2}$ = –83.1 $\pm$ 1.1 mV and a slope factor k = 9.9 $\pm$ 1.1 mV (n = 10).

There was considerable variation between bushy cells in the rates at which I_h activated and deactivated, suggesting that the subunit composition of the ion channels may differ among bushy cells. Rates of activation depended on voltage (Fig. 8*A*); activation rates were higher in responses to large than to small hyperpolarizations. Variation in the rate of activation of I_h among bushy cells is illustrated by the superposition of normalized current traces in responses to –112 mV (Fig. 8*E*). The activation of I_h required fitting with double exponentials, τ_f and τ_s. In most bushy cells rates varied between a, 40% τ_f 78 ms and 60% τ_s 410 ms, and b, 60% τ_f 56 ms and 40% τ_s 277 ms, but in one cell, *c*, I_h activated more quickly (Fig. 8*E*).

One of the features that make g_h biologically interesting is that its voltage-dependence is modulated by neurotransmitters. In cardiac and some neuronal cell types, including in T stellate cells of the VCN, I_h is modulated through a cAMP-dependent pathway (Banks et al. 1993; Leao et al. 2006; McCormick and Pape 1990a,b; Robinson and Siegelbaum 2003; Rodrigues and Oertel 2006), but in others, including octopus cells of the VCN the activation curves of which seem always to lie at the depolarizing extreme of the range of modulation, little modulation by cAMP was observed (Bal and Oertel 2000). Figure 9 (*A–C*) shows an example of the action of 500 μM 8-Br-cAMP, a membrane-permeable analogue of cAMP, on a bushy cell in which the activation curve shifted by ~6 mV. On average 500 μM 8-Br-cAMP caused a depolarizing shift in the half-activation voltage of I_h of 6.8 $\pm$ 1.8 mV (n = 4).

Temperature also affects I_h differently in different cells. In octopus cells, a reduction in temperature causes not only changes in kinetics, as expected, but also changes in the amplitude of I_h that adapt to the original level over a few minutes (Cao and Oertel 2005). In T stellate cells, a reduction

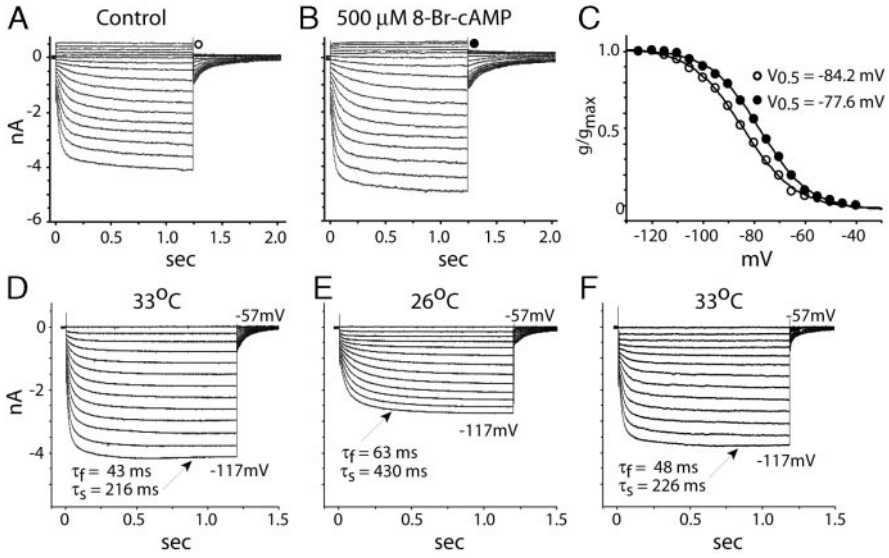

FIG. 9. In bushy cells I_h is modulated by cAMP (*A–C*) and by temperature (*D–F*). *A*: responses to a family of voltage pulses from a holding potential of −62 mV to conditioning voltages between −35 and −125 mV, and a test pulse to −77 mV reveals the typical pattern of activation of I_h. *B*: extracellular perfusion of 500 μM 8-Br-cAMP subtly changed g_h in the same cell. *C*: plots compare the voltage dependence of g_h, derived from tail currents as illustrated in Fig. 8*D* and normalized, in the absence (○) and presence (●) of 8-Br-cAMP. In this cell 8-Br-cAMP shifted $V_{0.5}$ by 6.6 mV in the positive direction. *D*: to determine how temperature affects the amplitude, kinetics, and voltage dependence, I_h was first measured at 33°C by holding the voltage at −57 mV, then stepping it to between −57 and −117 mV. *E*: temperature was then reduced to 26°C, and I_h was measured with a similar family of voltage pulses. Currents in responses to a step to −117 mV at the 2 temperatures were fitted with double-exponential functions showing that the time course of activation was slower at reduced temperature. The amplitude of currents was also reduced. The reduction in amplitude was stable; the traces shown in *E* were recorded 34 min after the temperature had been reduced. There was no difference in the voltage sensitivity of g_h. *F*: changes in I_h as a function of temperature were reversible. When the temperature was returned to 33°C, 7 min after the recording in *E,* the rate of activation and the magnitude of I_h had returned to near its original value.

in temperature reduces the rates of activation and deactivation and the amplitude, but in contrast with octopus cells, changes in amplitude are stable (Rodrigues and Oertel 2006). Figure 9 (*D–F*) shows that in bushy cells, too, the reduction in rate and amplitude was stable over time and that the voltage sensitivity was not altered by lowering the temperature from 33 to 26°C. In bushy cells, $V_{1/2}$ was −87.4 ± 2.3 mV at 33°C and −86.9 ± 1.8 mV at 26°C ($n = 4$).

Rate of depolarization (dV/dt) threshold

In every bushy cell tested, firing depended on the rate at which it was depolarized. Rapid depolarizations caused bushy cells to fire, whereas slow depolarizations did not. Each bushy cell has a threshold rate of depolarization that is independent of the magnitude of current when the current is suprathreshold (McGinley and Oertel 2006). Threshold rates of depolarization were measured by depolarizing bushy cells with currents that rose in ramps of varying amplitude. Measurements from three cells are illustrated in Fig. 10. For each ramp, the subthreshold rising phase of the voltage response was fit with a straight line the slope of which defined the d*V*/d*t* for that ramp (McGinley and Oertel 2006). Plots of the peak voltage reached during each ramp against the d*V*/d*t* revealed a step increase that was the threshold for firing in rate of depolarization (dV/dt_{thresh}; Fig. 10, *A–C*, panels on the *right*). In bushy cells, the dV/dt_{thresh} ranged from 1.4 to 4.2 mV/ms and had an average of 2.8 ± 0.5 mV/ms ($n = 18$).

Do biophysical properties define subclasses of bushy cells?

Expecting that mice might have globular and small spherical bushy cells and finding that their firing is correlated with position in the nucleus led us to question whether the biophysical properties of bushy cells fall into separate groups. An obvious difference between responses that were recorded with sharp electrodes and in the present group was in the firing of action potentials. Could bushy cells that fire more than two action potentials represent a population of more fragile bushy cells that was not represented in early sharp-electrode recordings? Figure 11 shows the relationship between the maximum number of action potentials fired by bushy cells and measurements of biophysical properties. The plots show that the bushy cells that fired fewest action potentials tended to have the largest maximal g_{KL}, the largest maximal g_h, the largest d*V*/d*t* threshold, the lowest input resistances, and the shortest τ_m. Maximum g_{KH} was not strongly correlated with repetitive firing. Most of the relationships do not show distinct breaks, but d*V*/d*t* thresholds do fall into two groups with bushy cells that fire only one or two action potentials having high rate thresholds and bushy cells that fire more than two action potentials having lower rate thresholds. Cluster analysis revealed that each of the relationships in Fig. 11 falls best into two groups as indicated by the ovals. In all panels except *B,* the populations delineated by the ovals were statistically significantly different from one another ($P < 0.05$, Student's *t*-test). Whether bushy cells fall into two distinct groups is unclear, however. On the one hand, there were only 3/86 measurements inconsistent with the conclusion that bushy cells fall into two groups, one that fired one or two action potentials and another more than two action potentials when depolarized with square current pulses. On the other hand, the finding that the groupings differed could indicate that the population of bushy cells forms a continuum.

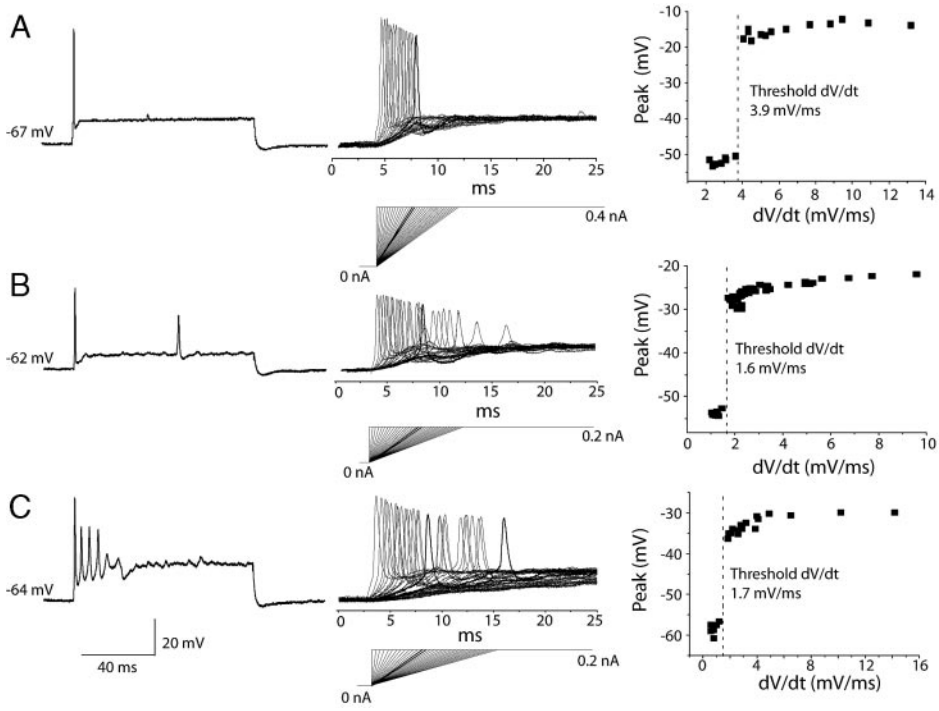

FIG. 10. Bushy cells have a threshold rate of depolarization for firing action potentials. Measurements in *A–C* show responses from separate bushy cells. *Left*: current steps evoke transient firing. *Middle*: ramps of current evoke firing only if they depolarize bushy cells faster than a threshold rate. The slowest suprathreshold ramp and corresponding voltage response and the fastest subthreshold ramp and its corresponding voltage response are indicated by thickened traces. *Right*: peak depolarization is plotted as a function of the slope of linear fits to the subthreshold rising phase of the voltage response to ramps of current (d*V*/d*t*). The firing of action potentials results in a jump in the peak voltage. The threshold d*V*/d*t* for each cell is shown with a dashed line. The threshold d*V*/d*t* ranged from 1.4 to 4.2 mV/ms and had an average of 2.8 ± 0.5 mV/ms ($n = 18$).

DISCUSSION

The present study confirms what had been reported incidentally (McGinley and Oertel 2006; Wang and Manis 2006): the criteria that were based on early recordings with sharp electrodes (Oertel 1983; Wu and Oertel 1984) were too narrow and excluded bushy cells that fire more action potentials at the onset of a depolarizing pulse. All bushy cells fired transiently when depolarized with current pulses; some bushy cells fired only once but others fired up to six action potentials. The g_{KL} that reduces repetitive firing was present in every anatomically identified bushy cell tested. Being partly activated at rest, g_{KL} and g_h affected the τ_m near rest that determines the shape of synaptic potentials; τ_m varied between 0.6 and 2 ms in the population of bushy cells we studied. The presence of g_{KL} distinguishes bushy cells from the T stellate cells in which g_{KL} is weak or absent (Ferragamo and Oertel 2002; Rodrigues and Oertel, unpublished results).

The present results are consistent with bushy cells forming two separate populations of cells, perhaps globular and small spherical bushy cells, but they are not definitive. The d*V*/d*t* thresholds of bushy cells clearly fell into two groups. Cluster analysis showed that other features, too, fell largely, but not entirely, into two groups, those that fired maximally one or two action potentials and those that fired maximally three or more action potentials when they were depolarized with current pulses. There was a trend for bushy cells near the nerve root to fire fewer action potentials when depolarized with current pulses, have shorter τ_m, and have higher d*V*/d*t* thresholds than those that lie more dorsal to the nerve root. The finding that there are significant differences between bushy cells is consistent with responses to tones in vivo. Responses to tones also differ among bushy cells. The "primary-like-with-notch" responses to tones of globular bushy cells show a sharp onset transient, whereas "primary-like" responses have a broader onset transient and their firing is more tonic but the differences

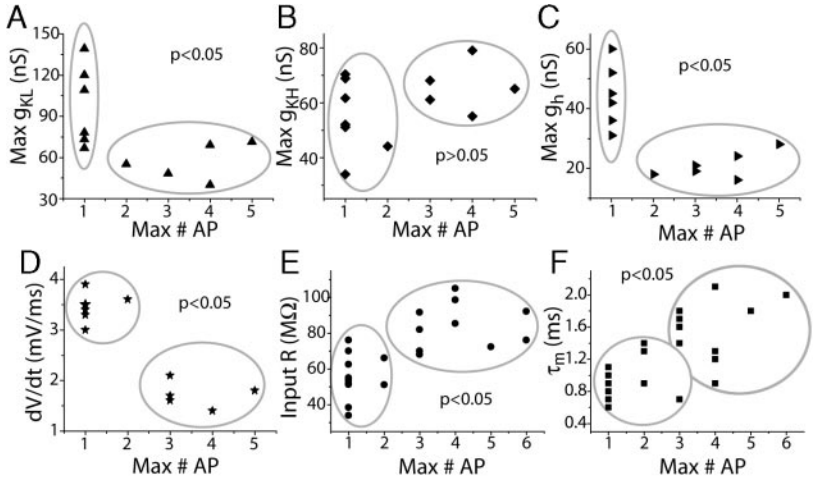

FIG. 11. To test whether the properties of bushy cells fall into 2 distinct groups or are continuously graded, biophysical characteristics are shown as a function of the maximum number of action potentials they fired in responses to depolarizing current steps. A–C: maximal g_{KL}, g_{KH}, and g_h are plotted as a function of the maximal number of action potentials. There was a strong correlation between maximal g_{KL} and g_h and firing, but there was only a weak correlation between maximal g_{KH} and maximal number of action potentials. *D*: bushy cells that fired few action potentials required faster depolarizations to generate action potentials than those that fired more action potentials. *E*: input resistance was measured as the slope of *V-I* plots at the resting potential. *F*: fall of voltage at the end of a small depolarization (response to 50 pA) was fit with a single exponential. The time constant of that fit, τ_m, is plotted on the ordinate. Cluster analysis was used to determine that data points optimally fell into 2 groups, indicated by the ovals. All groups except those in *B* differed significantly (Student's *t*-test, $P < 0.05$).

are sometimes subtle (Paolini et al. 2001; Rhode and Smith 1986; Smith et al. 1991; Winter and Palmer 1990). A high rate threshold enhances the sharpness of the onset transient in cells that sum many small inputs (Ferragamo and Oertel 2002; McGinley and Oertel 2006). If globular and small, spherical bushy cells differ biophysically, the present results suggest that globular bushy cells, more than small spherical bushy cells, are functionally specialized to detect the coincidence of multiple converging inputs. Incidental, but not systematic, estimates have been made of the number of converging auditory nerve fibers onto bushy cells in mice (Oertel 1985). In cats 6–69, but most often *15–23*, auditory nerve fibers converge on a globular bushy cell (Liberman 1993; Spirou et al. 2005). Also in cats it has been shown that large spherical bushy cells receive input through about three fibers (Brawer and Morest 1975). Corresponding measurements have, however, not been made in small spherical bushy cells.

Voltage-sensitive conductances in bushy cells follow a pattern that has been observed in many auditory neurons that are known to receive and convey information in the timing of firing. The combination of g_{KL} and g_{KH} was first documented in dissociated cells that might have been bushy cells (Manis and Marx 1991; Pal et al. 2005; Rothman and Manis 2003a–c) and then found in other cells including avian homologues of bushy cells (Rathouz and Trussell 1998; Reyes et al. 1994), primary auditory neurons (Mo and Davis 1997a; Mo et al. 2002), octopus cells of the mammalian VCN (Bal and Oertel 2001; Cao and Oertel 2005; Golding et al. 1995, 1999), identified bushy cells (Leao et al. 2004), principal cells of the MNTB (Brew and Forsythe 1995; Brew et al. 2003; Dodson et al. 2002; Forsythe and Barnes-Davies 1993; Kopp-Scheinpflug et al. 2003), ventral nucleus of the lateral lemniscus (Wu and Kelly 1995), MSO (Scott et al. 2005) and its avian homologue, nucleus laminaris (Kuba et al. 2002, 2005; Reyes et al. 1996), and LSO (Barnes-Davies et al. 2004). Synaptic terminals also have this combination of conductances (Dodson et al. 2003; Ishikawa et al. 2003). Most of these cells also contain g_h: primary auditory neurons (Chen 1997; Mo and Davis 1997b), octopus cells (Bal and Oertel 2000; Cao and Oertel 2005; Koch et al. 2004), bushy cells (Leao et al. 2005, 2006), MNTB neurons (Banks et al. 1993; Leao et al. 2005, 2006), ventral nucleus of the lateral lemniscus (Zhao and Wu 2001), MSO (Scott et al. 2005) and its avian homologue, nucleus laminaris (Reyes et al. 1996), and LSO (Barnes-Davies et al. 2004; Leao et al. 2006). I_h opposes I_{KL} at the resting potential.

Although the overall pattern is consistent, the magnitudes and some of the functional characteristics of the conductances in auditory neurons are surprisingly variable. For example, we have shown that on average g_{KLmax} is 80 nS in bushy cells but in octopus cells, the mean g_{KLmax} is 515 nS (Bal and Oertel 2001), and in young MNTB cells, it is reported to be 0.5 nS (Leao et al. 2004). In dissociated cells no I_h seems to have been detected (Manis and Marx 1991; Rothman and Manis 2003a). At reduced temperatures, the rates of activation and inactivation as well as the absolute magnitudes of g_{KL}, g_{KH}, and g_h are reduced differentially (Cao and Oertel 2005). In octopus cells, but not in bushy or T stellate cells, the magnitude of g_{hmax} adapts to a constant value when the temperature is altered (Cao and Oertel 2005; Leao et al. 2006; Rodrigues and Oertel 2006). Activity also has been reported to affect the expression of potassium channels (Lu et al. 2004). As neurons mature, the magnitude of g_h and g_{KL} grows several-fold in rodents between 1 and 3 wk after birth (Cuttle et al. 2001; Scott et al. 2005). In bushy cells, the magnitudes of both g_{hmax} and g_{KLmax} are correlated with the number of action potentials evoked by depolarizing current pulses. As blocking g_h does not affect firing, the correlation of g_{hmax} with firing could result from a requirement that I_h balances I_{KL} at rest to maintain a constant resting potential as it does in octopus cells (Oertel et al. 2000). Maturity also probably affects voltage sensitivity; for example in 2-wk-old mice, $V_{1/2}$ of g_h is reported to be –100 mV (Leao et al. 2005), whereas in 3-wk-old mice, we find it to be –83 mV. The voltage sensitivity varies within some of these cell populations (Mo and Davis 1997b). Measurements can also be affected by experimental parameters such as series resistance compensation (Rothman and Manis 2003a). Comparisons between populations of neurons are therefore most reliable within a study.

The presence of g_{KL} enhances the ability of auditory neurons to encode timing with temporal precision. First, this conductance gives neurons a low input resistance and a rapid τ_m that makes synaptic potentials brief and sharply timed (Kuba et al. 2005; Manis and Marx 1991; Mo and Davis 1997a; Oertel 1983; Reyes et al. 1996). The low input resistance leads to a requirement for large synaptic currents that are delivered either through large calyceal endings of individual fibers or through smaller endings of large numbers of fibers. Second, g_{KL} prevents repetitive firing (Barnes-Davies et al. 2004; Brew et al. 2003; Leao et al. 2004; Mo et al. 2002). Third, g_{KL} contributes to the repolarization not only of action potentials but also of synaptic potentials, sharpening their peaks (Kuba et al. 2005; Oertel et al. 2000; Scott et al. 2005). Fourth, it makes neurons sensitive to the rate at which they are depolarized (Ferragamo and Oertel 2002; McGinley and Oertel 2006). The larger the rate of depolarization that is required for firing, the more closely coincident subthreshold inputs need to be to contribute to firing (McGinley and Oertel 2006).

g_{KL} is mediated through K^+ channels of the Kv1 (also termed *shaker* or KCNA) family. In bushy cells, g_{KL} is blocked by α-DTX (present study; Leao et al. 2004), which, like DTX I (Lu et al. 2004; Rothman and Manis 2003a), blocks channels that contain Kv1.1, Kv1.2, Kv1.3, and Kv1.6 subunits (Dolly and Parcej 1996; Grissmer et al. 1994; Harvey 1997; Owen et al. 1997; Tytgat et al. 1995). Sensitivity of only 72% of I_{KL} to DTX-K, a toxin that blocks channels with a Kv1.1 subunit (Owen et al. 1997; Robertson et al. 1996; Wang et al. 1999a,b), and of only 58% of I_{KL} to tityustoxin Kα, a toxin that blocks channels with a Kv1.2 subunit (Hopkins 1998; Werkman et al. 1993), indicates that g_{KL} comprises a population of heteromeric channels of which not all contain Kv1.1 and not all contain Kv1.2 subunits, much as in octopus cells (Bal and Oertel 2001). mRNA and protein for Kv1.1 and Kv1.2 subunits are prominent in the AVCN (Grigg et al. 2000; Pal et al. 2005). In MNTB neurons of young rats, 95% of I_{KL} is sensitive to DTX-K, indicating that most channels contain Kv1.1 subunits (Dodson et al. 2003); I_{KL} is, however, reduced but not eliminated in mice that lack Kv1.1 subunits (Brew et al. 2003). In the MSO, too, a larger proportion of I_{KL} is sensitive to DTX-K than in bushy or octopus cells (Scott et al. 2005). g_{KL} is graded with tonotopy in some auditory nuclei (Barnes-Davies et al. 2004; Kuba et al. 2005), but no tonotopic gradient was ob-

served in the VCN in the magnitude of I_{KL} (present study) nor in the levels of Kv1 mRNA (Grigg et al. 2000).

The depolarized activation range of g_{KH} indicates that it is activated mainly by the peaks of action potentials and contributes to repolarizing them (Perney and Kaczmarek 1997; Rothman and Manis 2003c; Rudy et al. 1999; Rudy and McBain 2001; Wang et al. 1998); indeed blocking g_{KH} with TEA broadened action potentials in bushy cells. g_{KH} is likely mediated through channels that contain α subunits of the Kv3 (*shaw* or KCNC) family of potassium channels. mRNA for Kv3.1 and Kv3.3 is expressed in or near spherical and globular bushy cells (Grigg et al. 2000; Li et al. 2001; Perney and Kaczmarek 1997; Song et al. 2005; Weiser et al. 1994). In contrast with g_{KH} in bushy cells, half-activated at –17 mV and nearly completely inactivated after 5 s, Kv3.1 channels in *Xenopus* oocytes are half-activated at about +15 mV and inactivate only slightly over seconds (McCormack et al. 1990; Rudy et al. 1999; Weiser et al. 1994). Kv3.1 subunits are variable, however. They are alternatively spliced, allowing channels to be differentially targeted and differentially modulated by phosphorylation (Macica et al. 2003; Ponce et al. 1997; Song et al. 2005). Currents through Kv3.3 channels in *Xenopus* oocytes resemble I_{KH} in bushy cells more closely in that they inactivate strongly over seconds (Rudy and McBain 2001; Weiser et al. 1994). Furthermore, g_{KH} in bushy cells is similar to that in octopus cells (Bal and Oertel 2001); in the octopus cell area the mRNA for Kv3.1 subunit is expressed only weakly, whereas the mRNA for the Kv3.3 subunit is strongly expressed (Bal and Oertel 2001; Grigg et al. 2000; Li et al. 2001; Perney and Kaczmarek 1997). No tonotopic gradient has been observed in I_{KH} or in the expression of Kv3.1 or Kv3.3 mRNA in the VCN (Grigg et al. 2000). No A-type, high-voltage-activated current was detected in bushy cells in the present study, consistent with observations by Rothman and Manis (2003a) that type II cells do not have A-type K^+ currents.

Hyperpolarization-activated currents have a less direct role in signaling in bushy cells. Being activated at the resting potential, g_h contributes to setting the resting input conductance and I_h counteracts the resting I_{KL} in setting resting potential. In all VCN cells, the reversal potential of I_h was near –40 mV, but its voltage sensitivity and maximum amplitude varied between cell types under comparable conditions. In bushy cells, $V_{1/2}$ was relatively negative, –84 mV, so that a relatively small proportion of the conductance was activated at rest; it was even more negative, –88 mV, in T and D stellate cells, but much more positive, –65 mV, in octopus cells (Bal and Oertel 2000; Oertel and Fujino 2001; Rodrigues and Oertel 2006). The voltage sensitivity varies among primary auditory neurons (Mo and Davis 1997b). In bushy cells, g_{hmax} averaged ~30 nS, near the 20 nS average g_{hmax} in T stellate and 30 nS in D stellate cells but smaller than the 150 nS in octopus cells. Other authors have reported more negative values of $V_{1/2}$, –93 to –101 mV, and smaller g_{hmax}, 2–6 nS in bushy cells of 12- to 14-day-old mice (Leao et al. 2005, 2006). In bushy cells, as in other auditory neurons, blocking I_h did not significantly affect the shape of action potentials (Bal and Oertel 2000; Leao et al. 2006).

I_h is mediated through HCN (hyperpolarization-activated, cyclic nucleotide-gated) channels. HCN1 and HCN2 subunits are clearly present in the anterior VCN (Koch et al. 2004). It is unclear how strongly HCN3 and HCN4 are expressed in the brain stem; some authors report that they are expressed at low levels (Moosmang et al. 2001) and others that they are expressed at substantial levels (Leao et al. 2006; Monteggia et al. 2000). The sensitivity of I_h to cyclic nucleotides is common (DiFrancesco and Tortora 1991; Ludwig et al. 1998; McCormick and Pape 1990a; Pape and McCormick 1989; Santoro et al. 1998; Tokimasa and Akasu 1990; van Ginneken and Giles 1991). In bushy, stellate, and MNTB cells, cAMP shifts the voltage sensitivity of I_h in the depolarizing direction, depolarizing cells and thus increasing their excitability, whereas in octopus cells, the voltage sensitivity of I_h is already maximally depolarized (Bal and Oertel 2000; Banks et al. 1993; Oertel and Fujino 2001; Rodrigues and Oertel 2006).

ACKNOWLEDGMENTS

Several people made substantial contributions to this work. M. J. McGinley, J. H. Wittig Jr., and A. Rodrigues initially showed that multiple spiking cells have α-DTX-sensitive conductances. P. Chang did the cluster analysis for Fig. 11. We thank J. Doucet and D. Ryugo for valuable discussions. M. J. McGinley and E. Lenhart read the manuscript critically and made valuable suggestions. We are also fortunate to have expert help from staff members in the department. Most especially we thank R. Kochhar, who keeps our computers running smoothly and L. Barnes and other members of the office staff for administrative support.

GRANTS

This work was supported by National Institute of Deafness and Other Communications Disorders Grant DC-00176.

REFERENCES

Bal R, Oertel D. Hyperpolarization-activated, mixed-cation current (I_h) in octopus cells of the mammalian cochlear nucleus. *J Neurophysiol* 84: 806–817, 2000.

Bal R, Oertel D. Potassium currents in octopus cells of the mammalian cochlear nuclei. *J Neurophysiol* 86: 2299–2311, 2001.

Banks MI, Pearce RA, Smith PH. Hyperpolarization-activated cation current (I_h) in neurons of the medial nucleus of the trapezoid body: voltage-clamp analysis and enhancement by norepinephrine and cAMP suggest a modulatory mechanism in the auditory brain stem. *J Neurophysiol* 70: 1420–1432, 1993.

Barnes-Davies M, Barker MC, Osmani F, Forsythe ID. Kv1 currents mediate a gradient of principal neuron excitability across the tonotopic axis in the rat lateral superior olive. *Eur J Neurosci* 19: 325–333, 2004.

Brawer JR, Morest DK. Relations between auditory nerve endings and cell types in the cat's anteroventral cochlear nucleus seen with the Golgi method and Nomarski optics. *J Comp Neurol* 160: 491–506, 1975.

Brawer JR, Morest DK, Kane EC. The neuronal architecture of the cochlear nucleus of the cat. *J Comp Neurol* 155: 251–300, 1974.

Brew HM, Forsythe ID. Two voltage-dependent K^+ conductances with complementary functions in postsynaptic integration at a central auditory synapse. *J Neurosci* 15: 8011–8022, 1995.

Brew HM, Hallows JL, Tempel BL. Hyperexcitability and reduced low threshold potassium currents in auditory neurons of mice lacking the channel subunit Kv1.1. *J Physiol* 548: 1–20, 2003.

Brownell WE. Organization of the cat trapezoid body and the discharge characteristics of its fibers. *Brain Res* 94: 413–433, 1975.

Cant NB, Casseday JH. Projections from the anteroventral cochlear nucleus to the lateral and medial superior olivary nuclei. *J Comp Neurol* 247: 457–476, 1986.

Cant NB, Morest DK. Organization of the neurons in the anterior division of the anteroventral cochlear nucleus of the cat. Light-microscopic observations. *Neuroscience* 4: 1909–1923, 1979a.

Cant NB, Morest DK. The bushy cells in the anteroventral cochlear nucleus of the cat. A study with the electron microscope. *Neuroscience* 4: 1925–1945, 1979b.

Cao X, Oertel D. Temperature affects voltage-sensitive conductances differentially in octopus cells of the mammalian cochlear nucleus. *J Neurophysiol* 94: 821–832, 2005.

Chen C. Hyperpolarization-activated current (I_h) in primary auditory neurons. *Hear Res* 110: 179–190, 1997.

Cuttle MF, Rusznak Z, Wong AY, Owens S, Forsythe ID. Modulation of a presynaptic hyperpolarization-activated cationic current (I_h) at an excitatory synaptic terminal in the rat auditory brain stem. *J Physiol* 534: 733–744, 2001.

DiFrancesco D, Tortora P. Direct activation of cardiac pacemaker channels by intracellular cyclic AMP. *Nature* 351: 145–147, 1991.

Dodson PD, Barker MC, Forsythe ID. Two heteromeric Kv1 potassium channels differentially regulate action potential firing. *J Neurosci* 22: 6953–6961, 2002.

Dodson PD, Billups B, Rusznak Z, Szucs G, Barker MC, Forsythe ID. Presynaptic rat Kv1.2 channels suppress synaptic terminal hyperexcitability following action potential invation. *J Physiol* 550: 27–33, 2003.

Dolly JO, Parcej DN. Molecular properties of voltage-gated K^+ channels. *J Bioener Biomembr* 28: 231–253, 1996.

Doucet JR, Ryugo DK. Axonal pathways to the lateral superior olive labeled with biotinylated dextran amine injections in the dorsal cochlear nucleus of rats. *J Comp Neurol* 461: 452–465, 2003.

Ehret G. Age-dependent hearing loss in normal hearing mice. *Naturwissenschaften* 61: 506–507, 1974.

Ferragamo MJ, Oertel D. Octopus cells of the mammalian ventral cochlear nucleus sense the rate of depolarization. *J Neurophysiol* 87: 2262–2270, 2002.

Forsythe ID, Barnes-Davies M. The binaural auditory pathway: membrane currents limiting multiple action potential generation in the rat medial nucleus of the trapezoid body. *Phil Trans Roy Soc Lond B Biol Sci* 251: 143–150, 1993.

Francis HW, Manis PB. Effects of deafferentation on the electrophysiology of ventral cochlear nucleus neurons. *Hear Res* 149: 91–105, 2000.

Fujino K, Oertel D. Cholinergic modulation of stellate cells in the mammalian ventral cochlear nucleus. *J Neurosci* 21: 7372–7383, 2001.

Golding NL, Ferragamo MJ, Oertel D. Role of intrinsic conductances underlying responses to transients in octopus cells of the cochlear nucleus. *J Neurosci* 19: 2897–2905, 1999.

Golding NL, Robertson D, Oertel D. Recordings from slices indicate that octopus cells of the cochlear nucleus detect coincident firing of auditory nerve fibers with temporal precision. *J Neurosci* 15: 3138–3153, 1995.

Grigg JJ, Brew HM, Tempel BL. Differential expression of voltage-gated potassium channel genes in auditory nuclei of the mouse brainstem. *Hear Res* 140: 77–90, 2000.

Grissmer S, Nguyen AN, Aiyar J, Hanson DC, Mather RJ, Gutman GA, Karmilowicz MJ, Auperin DD, Chandy KG. Pharmacological characterization of five cloned voltage-gated K^+ channels, types Kv1.1, 1.2, 1.3, 1.5, and 3.1, stably expressed in mammalian cell lines. *Mol Pharmacol* 45: 1227–1234, 1994.

Harris NC, Constanti A. Mechanism of block by ZD 7288 of the hyperpolarization-activated inward rectifying current in guinea pig substantia nigra neurons in vitro. *J Neurophysiol* 74: 2366–2378, 1995.

Harvey AL. Recent studies on dendrotoxins and potassium ion channels. *Gen Pharmacol* 28: 7–12, 1997.

Hopkins WF. Toxin and subunit specificity of blocking affinity of three peptide toxins for heteromultimeric, voltage-gated potassium channels expressed in Xenopus oocytes. *J Pharmacol Exp Therapeut* 285: 1051–1060, 1998.

Ishikawa T, Nakamura Y, Saitoh N, Li W-B, Iwasaki S, Takahashi T. Distinct roles of Kv1 and Kv3 potassium channels at the calyx of Held presynaptic terminal. *J Neurosci* 23: 10445–10453, 2003.

Joris PX. Envelope coding in the lateral superior olive. II. Characteristic delays and comparison with responses in the medial superior olive. *J Neurophysiol* 76: 2137–2156, 1996.

Joris PX, Smith PH, Yin TC. Coincidence detection in the auditory system: 50 years after Jeffress. *Neuron* 21: 1235–1238, 1998.

Joris PX, Yin TC. Envelope coding in the lateral superior olive. I. Sensitivity to interaural time differences. *J Neurophysiol* 73: 1043–1062, 1995.

Kaczmarek LK, Bhattacharjee A, Desai R, Gan L, Song P, von Hehn CA, Whim MD, Yang B. Regulation of the timing of MNTB neurons by short-term and long-term modulation of potassium channels. *Hear Res* 206: 133–145, 2005.

Koch U, Braun M, Kapfer C, Grothe B. Distribution of HCN1 and HCN2 in rat auditory brain stem nuclei. *Eur J Neurosci* 20: 79–91, 2004.

Kopp-Scheinpflug C, Dehmel S, Dorrscheidt GJ, Rubsamen R. Interaction of excitation and inhibition in anteroventral cochlear nucleus neurons that receive large endbulb synaptic endings. *J Neurosci* 22: 11004–11018, 2002.

Kopp-Scheinpflug C, Fuchs K, Lippe WR, Tempel BL, Rubsamen R. Decreased temporal precision of auditory signaling in Kcna1-null mice: an electrophysiological study in vivo. *J Neurosci* 23: 9199–9207, 2003.

Kuba H, Koyano K, Ohmori H. Development of membrane conductance improves coincidence detection in the nucleus laminaris of the chicken. *J Physiol* 540: 529–542, 2002.

Kuba H, Yamada R, Fukui I, Ohmori H. Tonotopic specialization of auditory coincidence detection in nucleus laminaris of the chick. *J Neurosci* 25: 1924–34, 2005.

Leao KE, Leao RN, Sun H, Fyffe RE, Walmsley B. Hyperpolarization-activated currents are differentially expressed in mice brainstem auditory nuclei. *J Physiol* 576: 849–864, 2006.

Leao RN, Berntson A, Forsythe ID, Walmsley B. Reduced low-voltage activated K^+ conductances and enhanced central excitability in a congenitally deaf (dn/dn) mouse. *J Physiol* 559: 25–33, 2004.

Leao RN, Svahn K, Berntson A, Walmsley B. Hyperpolarization-activated (I) currents in auditory brain stem neurons of normal and congenitally deaf mice. *Eur J Neurosci* 22: 147–157, 2005.

Li W, Kaczmarek LK, Perney TM. Localization of two high-threshold potassium channel subunits in the rat central auditory system. *J Comp Neurol* 437: 196–218, 2001.

Liberman MC. Central projections of auditory-nerve fibers of differing spontaneous rate. I. Anteroventral cochlear nucleus. *J Comp Neurol* 313: 240–258, 1991.

Liberman MC. Central projections of auditory nerve fibers of differing spontaneous rate. II. Posteroventral and dorsal cochlear nuclei. *J Comp Neurol* 327: 17–36, 1993.

Lorente de No R. *The Primary Acoustic Nuclei.* New York: Raven, 1981.

Lu Y, Monsivais P, Tempel BL, Rubel EW. Activity-dependent regulation of the potassium channel subunits Kv1.1 and Kv3.1. *J Comp Neurol* 470: 93–106, 2004.

Ludwig A, Zong X, Jeglitsch M, Hofmann F, Biel M. A family of hyperpolarization-activated mammalian cation channels. *Nature* 393: 587–591, 1998.

Maccaferri G, McBain CJ. The hyperpolarization-activated current (I_h) and its contribution to pacemaker activity in rat CA1 hippocampal stratum oriens-alveus interneurons. *J Physiol* 497: 119–130, 1996.

Macica CM, von Hehn CA, Wang LY, Ho CS, Yokoyama S, Joho RH, Kaczmarek LK. Modulation of the kv3.1b potassium channel isoform adjusts the fidelity of the firing pattern of auditory neurons. *J Neurosci* 23: 1133–1141, 2003.

Manis PB, Marx SO. Outward currents in isolated ventral cochlear nucleus neurons. *J Neurosci* 11: 2865–2880, 1991.

McCormack T, Vega-Saenz de Miera EC, Rudy B. Molecular cloning of a member of a third class of Shaker-family K^+ channel genes in mammals. *Proc Natl Acad Sci USA* 87: 5227–5231, 1990.

McCormick DA, Pape HC. Noradrenergic and serotonergic modulation of a hyperpolarization-activated cation current in thalamic relay neurons. *J Physiol* 431: 319–342, 1990a.

McCormick DA, Pape HC. Properties of a hyperpolarization-activated cation current and its role in rhythmic oscillation in thalamic relay neurons. *J Physiol* 431: 291–318, 1990b.

McGinley MJ, Oertel D. Rate thresholds determine the precision of temporal integration in principal cells of the ventral cochlear nucleus. *Hear Res 216-217*: 52–63, 2006.

Mo ZL, Adamson CL, Davis RL. Dendrotoxin-sensitive K(+) currents contribute to accommodation in murine spiral ganglion neurons. *J Physiol* 542: 763–778, 2002.

Mo ZL, Davis RL. Endogenous firing patterns of murine spiral ganglion neurons. *J Neurophysiol* 77: 1294–1305, 1997a.

Mo ZL, Davis RL. Heterogeneous voltage dependence of inward rectifier currents in spiral ganglion neurons. *J Neurophysiol* 78: 3019–3027, 1997b.

Monteggia LM, Eisch AJ, Tang MD, Kaczmarek LK, Nestler EJ. Cloning and localization of the hyperpolarization-activated cyclic nucleotide-gated channel family in rat brain. *Mol Brain Res* 81: 129–139, 2000.

Moosmang S, Stieber J, Zong X, Biel M, Hofmann F, Ludwig A. Cellular expression and functional characterization of four hyperpolarization-activated pacemaker channels in cardiac and neuronal tissues. *Eur J Biochem* 268: 1646–1652, 2001.

Oertel D. Synaptic responses and electrical properties of cells in brain slices of the mouse anteroventral cochlear nucleus. *J Neurosci* 3: 2043–2053, 1983.

Oertel D. Use of brain slices in the study of the auditory system: spatial and temporal summation of synaptic inputs in cells in the anteroventral cochlear nucleus of the mouse. *J Acoust Soc Am* 78: 328–333, 1985.

Oertel D, Bal R, Gardner SM, Smith PH, Joris PX. Detection of synchrony in the activity of auditory nerve fibers by octopus cells of the mammalian cochlear nucleus. *Proc Nat Acad Sci USA* 97: 11773–11779, 2000.

Oertel D, Fujino K. Role of biophysical specialization in cholinergic modulation in neurons of the ventral cochlear nuclei. *Audiol Neurootol* 6: 161–166, 2001.

Oleskevich S, Clements J, Walmsley B. Release probability modulates short-term plasticity at a rat giant terminal. *J Physiol* 524: 513–523, 2000.

Oleskevich S, Walmsley B. Synaptic transmission in the auditory brainstem of normal and congenitally deaf mice. *J Physiol* 540: 447–455, 2002.

Osen KK. Cytoarchitecture of the cochlear nuclei in the cat. *J Comp Neurol* 136: 453–484, 1969.

Owen DG, Hall A, Stephens G, Stow J, Robertson B. The relative potencies of dendrotoxins as blockers of the cloned voltage-gated K^+ channel, mKv1.1 (MK-1), when stably expressed in Chinese hamster ovary cells. *Br J Pharmacol* 120: 1029–1034, 1997.

Pal B, Por A, Pocsai K, Szhcs G, Rusznak Z. Voltage-gated and background K^+ channel subunits expressed by the bushy cells of the rat cochlear nucleus. *Hear Res* 199: 57–70, 2005.

Paolini AG, FitzGerald JV, Burkitt AN, Clark GM. Temporal processing from the auditory nerve to the medial nucleus of the trapezoid body in the rat. *Hear Res* 159: 101–116, 2001.

Pape HC, McCormick DA. Noradrenaline and serotonin selectively modulate thalamic burst firing by enhancing a hyperpolarization-activated cation current. *Nature* 340: 715–718, 1989.

Perney TM, Kaczmarek LK. Localization of a high threshold potassium channel in the rat cochlear nucleus. *J Comp Neurol* 386: 178–202, 1997.

Ponce A, Vega-Saenz dM, Kentros C, Moreno H, Thornhill B, Rudy B. K^+ channel subunit isoforms with divergent carboxy-terminal sequences carry distinct membrane targeting signals. *J Membr Biol* 159: 149–159, 1997.

Rathouz M, Trussell L. Characterization of outward currents in neurons of the avian nucleus magnocellularis. *J Neurophysiol* 80: 2824–2835, 1998.

Reyes AD, Rubel EW, Spain WJ. Membrane properties underlying the firing of neurons in the avian cochlear nucleus. *J Neurosci* 14: 5352–5364, 1994.

Reyes AD, Rubel EW, Spain WJ. In vitro analysis of optimal stimuli for phase-locking and time-delayed modulation of firing in avian nucleus laminaris neurons. *J Neurosci* 16: 993–1007, 1996.

Rhode WS, Oertel D, Smith PH. Physiological response properties of cells labeled intracellularly with horseradish peroxidase in cat ventral cochlear nucleus. *J Comp Neurol* 213: 448–463, 1983.

Rhode WS, Smith PH. Encoding timing and intensity in the ventral cochlear nucleus of the cat. *J Neurophysiol* 56: 261–286, 1986.

Robertson B, Owen D, Stow J, Butler C, Newland C. Novel effects of dendrotoxin homologues on subtypes of mammalian Kv1 potassium channels expressed in *Xenopus* oocytes. *FEBS Lett* 383: 26–30, 1996.

Robinson RB, Siegelbaum SA. Hyperpolarization-activated cation currents: from molecules to physiological function. *Annu Rev Physiol* 65: 453–480, 2003.

Rodrigues ARA, Oertel D. Hyperpolarization-activated currents regulate excitability in stellate cells of the mammalian ventral cochlear nucleus. *J Neurophysiol* 95: 76–87, 2006.

Rothman JS, Manis PB. Differential expression of three distinct potassium currents in the ventral cochlear nucleus. *J Neurophysiol* 89: 3070–3082, 2003a.

Rothman JS, Manis PB. Kinetic analyses of three distinct potassium conductances in ventral cochlear nucleus neurons. *J Neurophysiol* 89: 3083–3096, 2003b.

Rothman JS, Manis PB. The roles potassium currents play in regulating the electrical activity of ventral cochlear nucleus neurons. *J Neurophysiol* 89: 3097–3113, 2003c.

Rudy B, Chow A, Lau D, Amarillo Y, Ozaita A, Saganich M, Moreno H, Nadal MS, Hernandez-Pineda R, Hernandez-Cruz A, Erisir A, Leonard C, Vega-Saenz de Miera E. Contributions of Kv3 channels to neuronal excitability. *Ann NY Acad Sci* 868: 304–343, 1999.

Rudy B, McBain CJ. Kv3 channels: voltage-gated K^+ channels designed for high-frequency repetitive firing. *Trends Neurosci* 24: 517–526, 2001.

Santoro B, Liu DT, Yao H, Bartsch D, Kandel ER, Siegelbaum SA, Tibbs GR. Identification of a gene encoding a hyperpolarization-activated pacemaker channel of brain. *Cell* 93: 717–729, 1998.

Schwarz DW, Puil E. Firing properties of spherical bushy cells in the anteroventral cochlear nucleus of the gerbil. *Hear Res* 114: 127–138, 1997.

Scott LL, Mathews PJ, Golding NL. Posthearing developmental refinement of temporal processing in principal neurons of the medial superior olive. *J Neurosci* 25: 7887–7895, 2005.

Sento S, Ryugo DK. Endbulbs of held and spherical bushy cells in cats: morphological correlates with physiological properties. *J Comp Neurol* 280: 553–562, 1989.

Shin KS, Rothberg BS, Yellen G. Blocker state dependence and trapping in hyperpolarization-activated cation channels: evidence for an intracellular activation gate. *J Gen Physiol* 117: 91–101, 2001.

Smith PH, Joris PX, Carney LH, Yin TC. Projections of physiologically characterized globular bushy cell axons from the cochlear nucleus of the cat. *J Comp Neurol* 304: 387–407, 1991.

Smith PH, Joris PX, Yin TC. Projections of physiologically characterized spherical bushy cell axons from the cochlear nucleus of the cat: evidence for delay lines to the medial superior olive. *J Comp Neurol* 331: 245–260, 1993.

Smith PH, Rhode WS. Characterization of HRP-labeled globular bushy cells in the cat anteroventral cochlear nucleus. *J Comp Neurol* 266: 360–375, 1987.

Song P, Yang Y, Barnes-Davies M, Bhattacharjee A, Hamann M, Forsythe ID, Oliver DL, Kaczmarek LK. Acoustic environment determines phosphorylation state of the Kv3.1 potassium channel in auditory neurons. *Nat Neurosci* 8: 1335–1342, 2005.

Spirou GA, Brownell WE, Zidanic M. Recordings from cat trapezoid body and HRP labeling of globular bushy cell axons. *J Neurophysiol* 63: 1169–1190, 1990.

Spirou GA, Rager J, Manis, PB. Convergence of auditory nerve fiber projections onto globular bushy cells. *Soc Neurosci Abstr* 44.7, 2005.

Tokimasa T, Akasu T. Cyclic AMP regulates an inward rectifying sodium-potassium current in dissociated bull-frog sympathetic neurones. *J Physiol* 420: 409–429, 1990.

Tolbert LP, Morest DK. The neuronal architecture of the anteroventral cochlear nucleus of the cat in the region of the cochlear nerve root: electron microscopy. *Neuroscience* 7: 3053–3067, 1982a.

Tolbert LP, Morest DK. The neuronal architecture of the anteroventral cochlear nucleus of the cat in the region of the cochlear nerve root: Golgi and Nissl methods. *Neuroscience* 7: 3013–3030, 1982b.

Tolbert LP, Morest DK, Yurgelun-Todd DA. The neuronal architecture of the anteroventral cochlear nucleus of the cat in the region of the cochlear nerve root: horseradish peroxidase labelling of identified cell types. *Neuroscience* 7: 3031–3052, 1982.

Tollin DJ, Yin TC. Interaural phase and level difference sensitivity in low-frequency neurons in the lateral superior olive. *J Neurosci* 25: 10648–10657, 2005.

Tytgat J, Debont T, Carmeliet E, Daenens P. The alpha-dendrotoxin footprint on a mammalian potassium channel. *J Biol Chem* 270: 24776–24781, 1995.

van Ginneken AC, Giles W. Voltage clamp measurements of the hyperpolarization-activated inward current I(f) in single cells from rabbit sino-atrial node. *J Physiol* 434: 57–83, 1991.

Wang FC, Bell N, Reid P, Smith LA, McIntosh P, Robertson B, Dolly JO. Identification of residues in dendrotoxin K responsible for its discrimination between neuronal K^+ channels containing Kv1.1 and 1.2 alpha subunits. *Eur J Biochem* 263: 222–229, 1999a.

Wang FC, Parcej DN, Dolly JO. alpha subunit compositions of Kv1.1-containing K^+ channel subtypes fractionated from rat brain using dendrotoxins. *Eur J Biochem* 263: 230–237, 1999b.

Wang LY, Gan L, Forsythe ID, Kaczmarek LK. Contribution of the Kv3.1 potassium channel to high-frequency firing in mouse auditory neurons. *J Physiol* 509: 183–194, 1998.

Wang Y, Manis PB. Temporal coding by cochlear nucleus bushy cells in DBA/2J mice with early onset hearing loss. *J Assoc Res Otolaryngol* 7: 412–424, 2006.

Weiser M, Vega-Saenz dM, Kentros C, Moreno H, Franzen L, Hillman D, Baker H, Rudy B. Differential expression of Shaw-related K^+ channels in the rat central nervous system. *J Neurosci* 14: 949–972, 1994.

Werkman TR, Gustafson TA, Rogowski RS, Blaustein MP, Rogawski MA. Tityustoxin-K alpha, a structurally novel and highly potent K^+ channel peptide toxin, interacts with the alpha-dendrotoxin binding site on the cloned Kv1.2 K^+ channel. *Mol Pharmacol* 44: 430–436, 1993.

Willard FH, Ryugo DK. Anatomy of the central auditory system. In: *The Auditory Psychobiology of the Mouse*, edited by Willott JF. Springfield, IL: Charles C Thomas, 1983, p. 201–304.

Winter IM, Palmer AR. Responses of single units in the anteroventral cochlear nucleus of the guinea pig. *Hear Res* 44: 161–178, 1990.

Wu SH. Physiological properties of neurons in the ventral nucleus of the lateral lemniscus of the rat: intrinsic membrane properties and synaptic responses. *J Neurophysiol* 81: 2862–2874, 1999.

Wu SH, Kelly JB. In vitro brain slice studies of the rat's dorsal nucleus of the lateral lemniscus. I. Membrane and synaptic response properties. *J Neurophysiol* 73: 780–793, 1995.

Wu SH, Oertel D. Intracellular injection with horseradish peroxidase of physiologically characterized stellate and bushy cells in slices of mouse anteroventral cochlear nucleus. *J Neurosci* 4: 1577–1588, 1984.

Yin TCT. Neural mechanisms of encoding binaural localization cues in the auditory brain stem. In: Integrative Functions in the Mammalian Auditory Pathway, edited by Oertel D, Fay RR and Popper AN. NY: Springer, p. 99–159, 2002.

Zhang S, Oertel D. Cartwheel and superficial stellate cells of the dorsal cochlear nucleus of mice: intracellular recordings in slices. *J Neurophysiol* 69: 1384–1397, 1993.

Zhang S, Trussell LO. Voltage clamp analysis of excitatory synaptic transmission in the avian nucleus magnocellularis. *J Physiol* 480: 123–136, 1994.

Zhao M, Wu SH. Morphology and physiology of neurons in the ventral nucleus of the lateral lemniscus in rat brain slices. *J Comp Neurol* 433: 255–271, 2001.